See published version at **https://doi.org/10.1016/j.ymthe.2020.12.009**

TITLE: Microglial vesicles improve post-stroke recovery by preventing immune cell senescence and favoring oligodendrogenesis

Stefano Raffaele [1], Paolo Gelosa [2], Elisabetta Bonfanti [1], Marta Lombardi [3], Laura Castiglioni [4], Mauro Cimino [5], Luigi Sironi [2,4], Maria P. Abbracchio [1], Claudia Verderio [3], Marta Fumagalli [1,*]

1 Department of Pharmacological and Biomolecular Sciences, Università degli Studi di Milano, 20133 Milan, Italy

2 IRCCS Centro Cardiologico Monzino, 20138 Milan, Italy

3 CNR Institute of Neuroscience, 20129 Milan, Italy

4 Department of Pharmaceutical Sciences, Università degli Studi di Milano, 20133 Milan, Italy

5 Department of Biomolecular Sciences, Università degli Studi di Urbino, 61029 Urbino, Italy

* Corresponding author. E-mail: marta.fumagalli@unimi.it

Running Title

Microglia-OPC crosstalk after stroke

See published version at **https://doi.org/10.1016/j.ymthe.2020.12.009**

Abstract

Contrasting myelin damage through the generation of new myelinating oligodendrocytes represents a promising approach to promote functional recovery after stroke. Here, we asked whether activation of microglia and monocyte-derived macrophages affects the regenerative process sustained by GPR17-expressing oligodendrocyte precursor cells (OPCs), a subpopulation of OPCs specifically reacting to ischemic injury. GPR17-iCreER^{T2}:CAG-eGFP reporter mice were employed to trace the fate of GPR17-expressing (GFP^{+}) OPCs after permanent middle cerebral artery occlusion. By microglia/macrophages pharmacological depletion studies, we show that innate immune cells favour GFP^{+} OPCs reaction and limit myelin damage early after injury, while they lose their pro-resolving capacity and acquire a dystrophic "senescent-like" phenotype at later stages. Intracerebral infusion of regenerative microglia-derived extracellular vesicles (EVs) restores protective microglia/macrophages functions, limiting their senescence during the post-stroke phase, and enhances the maturation of GFP^{+} OPCs at lesion borders, resulting in ameliorated neurological functionality. *In vitro* experiments show that EV-carried transmembrane TNFα mediates the pro-differentiating effects on OPCs, with future implications for regenerative therapies.

Keywords

Cerebral ischemia/Extracellular vesicles/GPR17 receptor/Microglia/Oligodendrocyte precursor cells

Introduction

Ischemic stroke is a neurological disease of cardiovascular origin that still remains a leading cause of death and permanent disability worldwide.[1] Early ischemic damage is triggered by the interruption of blood supply to a specific area of the brain and affects not only neurons but also oligodendrocytes, the myelin forming glial cells enwrapping neuronal axons and ensuring impulse transmission. The resulting loss of oligodendrocyte integrity contributes to the axonal degeneration and long-term functional and cognitive deficits observed after stroke.[2,3] Current therapy is limited to thrombolysis which has, however, a narrow treatment window and high risk of cerebral hemorrhage.[4] Thus, new strategies aimed at enhancing endogenous myelin repair, through the repopulation of myelin-forming oligodendrocytes, represent promising therapeutic perspectives to improve functional recovery after stroke.[5–8] On top of this, agents or approaches improving recovery in stroke models like permanent middle cerebral artery occlusion (MCAo), are believed to prove efficacious also in other neurodegenerative conditions characterized by neuronal disfunction and myelin deterioration associated to neurological and cognitive defects.[9]

Upon a demyelinating injury, the oligodendrocyte precursor cells (OPCs) present in the adult brain parenchyma migrate to the lesion site, proliferate and differentiate to myelinating oligodendrocytes.[10,11] Specifically, fate mapping studies using the conditional reporter mouse line GPR17-iCreER^{T2}:CAG-eGreen fluorescent protein (GFP) revealed that the subpopulation of OPCs expressing the P2Y-like receptor GPR17, which is permanently labelled by GFP upon tamoxifen-induced recombination, constitutes a reserve pool persisting in the adult rodent brain for repair purposes.[12] Due to the transient expression of GPR17, that is highest at the pre-oligodendrocyte stage and then disappears in fully-differentiated oligodendrocytes,[13]

these transgenic reporter mice represent the only means to study *in vivo* the role of GPR17 in OPC differentiation. Tamoxifen-induced recombination in this mouse line indeed results in the permanent labelling of the OPCs that express GPR17 at the very moment of tamoxifen administration; fluorescent labeling persists even after GPR17 downregulation and is also transmitted to cells progeny, thus allowing cells' terminal maturation.[12] By exploiting GPR17-iCreER^{T2}:CAG-eGFP mice, it has been demonstrated that this pool of cells (hereafter referred to as GPR17-expressing or GFP^{+} OPCs) actively reacts to ischemic damage by increasing their proliferation rate and migratory ability in order to accumulate at injury borders.[14] However, the spontaneous maturation capabilities of GFP^{+} OPCs recruited at the site of damage appear very limited.[14] Data coming from experimental models of multiple sclerosis highlight the importance of a permissive local environment for the maturation of this pool of progenitors.[15,16] Thus, the remyelination failure observed after the initial reaction of these precursors to ischemic damage may be due to the unfavorable local inflammatory milieu, which is mainly sustained by brain resident microglia and blood-borne macrophages.[17] However, the role of microglia/macrophages after stroke is very complex, since these cells are able not only to limit but also to aid repair mechanisms.[18] At early stages after ischemic injury, microglia exert protective functions by containing detrimental astrocyte activation,[19] by limiting neutrophil infiltration within the lesion,[20] and by reducing excitotoxic injury to neurons.[21] On the contrary, at later time points microglia/macrophages acquire a detrimental pro-inflammatory phenotype hindering brain repair processes.[18,22] Pharmacological modulation of microglial polarization could influence oligodendrogenesis and OPC differentiation, improving fiber connectivity and long-term functional recovery after stroke.[7,8] Furthermore, pro-regenerative microglia have been shown to support

remyelination in other experimental models of neurodegenerative disorders such as multiple sclerosis[23] and Alzheimer's disease.[24]

Growing evidence indicates novel mechanisms through which immune cells can influence the response of neighboring cells in the brain. Recent studies have attributed to extracellular vesicles (EVs) the capability to mediate intercellular exchanges among brain cells.[25] Specifically, microglia utilize EVs to regulate the level of synaptic proteins in recipient neurons,[26] to control migration and maturation of OPCs[27] or to propagate inflammatory and degenerative signals in response to tissue damage and disease.[28–30] Of note, the molecular composition and function of microglial EVs reflects the activation state of donor cells.[31] While EVs derived from inflammatory microglia have been shown to block remyelination, EVs produced by pro-regenerative cells efficiently promoted myelin repair,[27] thus emerging as promising tools to foster regenerative processes following brain injuries. However, how microglia/macrophages orchestrate the response of the pool of GPR17-expressing OPCs following ischemic stroke, as well as the specific impact of microglia-derived EVs in this process, have never been explored.

In this study, we investigated the contribution of microglia/macrophages to the response of GPR17-expressing OPCs after ischemic stroke, using GPR17-iCreER^{T2}:CAG-eGFP reporter mice subjected to MCAo. We demonstrate that microglia/macrophages exert a beneficial action on GPR17-expressing OPCs (i.e. GFP$^+$ OPCs) in the early injury phase after MCAo, while their activation becomes detrimental at later stage. Importantly, we show that infusion of EVs derived from pro-regenerative microglia favors a pro-resolving phenotype and rescue dystrophic, senescent-like traits of resident immune cells, leading to GFP$^+$ OPC differentiation and increased functional recovery. Finally, we provide initial clues of the involvement

of transmembrane tumor necrosis factor-α (tmTNFα) in the mechanism underlying the beneficial effect of microglial EVs on OPC maturation.

Results

Activation of microglia/macrophages increases over time after cerebral ischemia

To characterize microglia/macrophage activation in GPR17-iCreER^{T2}:CAG-eGFP reporter mice after cerebral ischemia, we performed immunohistochemistry (IHC) analysis for the microglial/macrophagic marker Iba1 at ischemic lesion boundaries (0-500 μm from the lesion border) and in the corresponding region of the intact contralateral hemisphere at day 1, 3, 7, and 14 post-MCAo (Fig 1A). Starting from day 3 post-MCAo, a statistically significant increase in Iba1-expressing (Iba1$^+$) cell density at the boundary of ischemic lesion was found compared to the corresponding region of the intact contralateral hemisphere (Fig 1B, E). Moreover, Iba1$^+$ cells continued to accumulate at injury borders up to day 14 post-MCAo (Fig 1B, E). Notably, at both day 3 and day 14 post-MCAo, the majority of Iba1$^+$ cells co-expressed the scavenger receptor CD68 (Fig S1), indicating ongoing phagocytic activity. In particular, at day 3 post-MCAo, CD68 expression was diffused in the whole cell body, while, at day 14 post-MCAo, CD68 was mainly detectable in defined intracellular structures reminiscent of phagolysosomes, suggesting different phases of the phagocytic process taking place during the early or late stage after ischemia (Fig S1).

Microglia/macrophage activation was also characterized by progressive morphological modifications (Fig 1B and S1), exhibiting highly ramified resting structure in the healthy contralateral hemisphere and hypertrophic and ameboid shape in the ipsilateral hemisphere starting from day 3 post-MCAo, reflecting intense

inflammatory activity.[32] Of note, at day 14 post-MCAo, Iba1$^+$ cells acquired a dystrophic morphology with fragmented cell processes and reduced cell volume (Fig 1B and S1), reminiscent of senescent-like cells.[32] Microglia/macrophage activation was paralleled by the increase of GPR17-expressing OPCs, labelled by GFP expression (GFP$^+$ cells), at injury borders (Fig S2), consistent with stroke-induced GFP$^+$ cell proliferation and migration.[14] A statistically significant positive correlation between Iba1$^+$ and GFP$^+$ cell densities was found, suggesting a possible functional inter-relationship between these two cell subsets (Fig S2).

Although it is known that microglia/macrophages are able to acquire a broad spectrum of activation states resulting in a variety of immune-phenotypes,[33,34] specific cell markers are useful to get information on detrimental phenotype, e.g. Fc gamma receptors CD16/32, and pro-regenerative status, e.g. chitinase 3-like 3, Ym1.[35,36] On this basis, we performed Iba1 co-staining with CD16/32 or Ym1 to quantify pro-inflammatory and pro-regenerative cells, respectively. At the border of ischemic lesion, pro-inflammatory cells co-expressing Iba1 and CD16/32 sharply increased over time up to day 14 post-MCAo (Fig 1C, F and Fig S3), while the number of pro-regenerative cells, double positive for Iba1 and Ym1, after an initial increase at day 3 post-MCAo, remained constant (Fig 1D, G and Fig S3). Interestingly, at day 3 post-MCAo, a considerable fraction of Iba1$^+$ cells co-expressed both CD16/32 and Ym1 (Fig S3).

Taken together, these results delineated two distinct temporal windows in the cellular response following MCAo, namely an early phase (day 3 post-MCAo), when hypertrophic pro-inflammatory and pro-regenerative Iba1$^+$ cells coexist at the border of the ischemic lesion, and a late stage (day 14 post-MCAo), when dystrophic, senescent-like, pro-inflammatory cells dominate the peri-infarct area.

At early stages after ischemia, microglia/macrophages exert beneficial effects on the response of GPR17-expressing OPCs

Our initial characterization data suggest that microglia/macrophages exert differential effects depending on the phenotype that they acquire at different times of ischemic progression. To evaluate the impact of microglia/macrophages on GFP^+ OPC response after MCAo, we exploited a previously described approach based on the administration of gadolinium chloride ($GdCl_3$), a cytotoxic agent capable to specifically induce apoptosis of phagocytic myeloid cells.[23,37] GPR17-iCreER^{T2}:CAG-eGFP reporter mice were treated with four daily intranasal administrations of $GdCl_3$ starting from 2 hours before MCAo (Fig 2A). At day 3 post-MCAo, a partial but statistically significant reduction of $Iba1^+$ cell density was observed at the border of the ischemic lesion in $GdCl_3$-treated animals compared to those receiving vehicle (Fig 2B, C), suggesting that this cytotoxin was able to induce a partial microglia/macrophages depletion during the early phase after ischemia. This treatment was equally effective in depleting both $Iba1^+$&$CD16/32^+$ pro-inflammatory, and $Iba1^+$&$Ym1^+$ pro-regenerative cells (Fig 2B, C and Fig S4). Interestingly, the early partial depletion of microglia/macrophages was paralleled by a significant reduction of GFP^+ OPC density, mainly affecting early precursors co-expressing NG2, at the border of the ischemic lesion (Fig 2B, D and Fig S5). The percentage of $GFP^+/Olig2^+$ on the total $Olig2^+$ oligodendroglial population is, instead, the same in mice treated with vehicle or $GdCl_3$ (Fig S5), excluding variations in GFP expression. Of note, the decrease of early GFP^+ OPC density may be due to impaired microglia-dependent proliferation of these cells, as also suggested by the smaller percentage of GFP^+ OPCs incorporating 5-bromo-2′-deoxyuridine (BrdU) observed in $GdCl_3$-

treated animals as compared to vehicle group (Fig 2B, D). Accordingly, a positive linear correlation between the density of $Iba1^+$ and GFP^+ cells was found at this time point (Fig 2E). Importantly, no changes in propidium iodide-stained cells were detected after exposure of primary OPC cultures to $GdCl_3$ (Fig S5), thus excluding direct oligo-toxicity of this compound. In addition, damage to myelin structure was exacerbated upon the partial depletion of microglia/macrophages during the early phase after MCAo, as indicated by increased g-ratio and reduction of both myelin thickness and myelinated axon density in the corpus callosum of $GdCl_3$-treated animals as compared to vehicle-treated littermates (Fig 2F, G). Conversely, no significant changes in axon diameter were detected between vehicle and $GdCl_3$ groups (Fig 2F, G), excluding a direct effect of early microglia/macrophages reduction also on axonal integrity. Taken together, these results suggest that, during the early phase after cerebral ischemia, microglia/macrophages are beneficial for the response of GPR17-expressing OPCs and contribute to limiting myelin damage.

At later stages after ischemia, the partial depletion of microglia/macrophages increases the response of GPR17-expressing OPCs, but has no impact on their maturation

To achieve microglia/macrophage depletion at later stages after cerebral ischemia, when pro-inflammatory cells dramatically increase at injury borders, GPR17-$iCreER^{T2}$:CAG-eGFP reporter mice received four daily doses of $GdCl_3$ starting from day 14 post-MCAo (Fig 3A). At day 17 post-MCAo, $GdCl_3$ treatment was able to partially but significantly reduce $Iba1^+$ cell density in the ischemic penumbra (Fig 3B, C). At this time point, $GdCl_3$ treatment depleted only $Iba1^+$&$CD16/32^+$ pro-inflammatory microglia/macrophages, while $Iba1^+$&$Ym1^+$ pro-regenerative cells were

not affected (Fig 3B, C and Fig S4). Under these conditions, we found a statistically significant increase in the density of GFP^+ OPCs at the border of the ischemic lesion, compared to vehicle-treated animals (Fig 3B, D), and a negative correlation between the densities of $Iba1^+$ and GFP^+ cells (Fig 3E). It is worth noting that, despite strong reactive astrogliosis is commonly reported after microglia depletion approaches,[19,38] no changes in GFAP immunoreactivity were detected following $GdCl_3$ administration at both early and late stages after MCAo (Fig S5). To analyse the impact of the late partial depletion of microglia/macrophages on long-term GFP^+ OPC differentiation, an additional experimental group was sacrificed at day 42 post-MCAo, four weeks after treatment with $GdCl_3$ or vehicle (Fig 3A). Results show that the increase in the density of GFP^+ OPCs was maintained in $GdCl_3$-treated animals also at this time point, but that the differentiation capability of these cells did not improve, as no differences in the percentage of GFP^+ cells co-expressing the mature oligodendroglial marker GSTπ were detected (Fig 3F, G). Accordingly, myelin density in the ipsilateral corpus callosum was not affected by late microglia/macrophages depletion (Fig 3H, I). These results indicate that, at late stages after MCAo, the pharmacological depletion of pro-inflammatory $Iba1^+$ cells could improve the capacity of GFP^+ OPCs to stack at injury borders but was not able to ameliorate their terminal maturation.

Infusion of microglia-derived extracellular vesicles modifies the phenotype of microglia/macrophages at lesion borders

Based on the data described above, we reasoned that reprogramming dystrophic and pro-inflammatory microglia/macrophages could be useful to enhance tissue remodeling and functional recovery after cerebral ischemia. Very relevant, microglial EVs have been shown to modify the phenotype and morphology of recipient

microglia/macrophages *in vivo*,[28] with different final effects depending on the activation state of the donor cells.[39,40] On this basis, EVs collected from *in vitro* manipulated pro-regenerative (IL-4 EVs) or pro-inflammatory (i-EVs) microglia were infused into the ipsilateral corpus callosum of GPR17-iCreER^{T2}:CAG-eGFP reporter mice through osmotic minipumps, starting from day 14 post-MCAo and allowing chronic delivery for 1 week (Fig 4A and S6). Tunable Resistive Pulse Sensing (TRPS) technique showed no statistically significant differences in EVs concentration and size distribution between i-EVs and IL-4 EVs (Fig S6). IHC analysis was performed at day 28 post-MCAo to evaluate the impact of the infusion of microglial EVs on resident microglia/macrophages in the peri-infarct region. Results show no variations in global Iba1$^+$ cell density after infusion of either IL-4 EVs, i-EVs or vehicle alone (Fig 4B-D). A slight but significative increase was detected in the density of pro-inflammatory cells co-expressing Iba1 and CD16/32 after infusion of i-EVs as compared to vehicle administration (Fig 4B, D). The density of Iba1$^+$&Ym1$^+$ pro-regenerative microglia/macrophages was instead found to be higher after infusion of IL-4 EVs compared to i-EVs and vehicle treatment (Fig 4C, D). Moreover, morphological analysis revealed that both IL-4 EVs and i-EVs induced prominent modifications of Iba1$^+$ cell branching when compared to vehicle-treated animals. Namely, an increase in the number of branchpoints and ramification index (Fig 4E), indicative of a recovery from a dystrophic shape to a functional one,[32] was observed. In addition, exposure to IL-4 EVs resulted in markedly increased Iba1$^+$ cell volume and surveilled cell territory compared to vehicle and i-EVs (Fig 4E), which is coherent with a switch towards pro-resolving functions. Globally, these data suggest that IL-4 EV infusion had a significant impact on microglia/macrophages at injury boundaries, promoting their pro-regenerative activation.

Infusion of pro-regenerative microglia-derived extracellular vesicles promotes GPR17-expressing OPC maturation after cerebral ischemia

In addition to the aforementioned effects of microglial EVs on Iba1$^+$ cells, our recent evidence indicates that EVs produced by microglia are also able to directly influence OPCs surrounding myelin lesions.[27] Thus, we analyzed the impact of microglia-derived EVs infusion on the differentiation of GPR17-expressing OPCs, labelled by GFP expression, in the peri-infarct area.

At day 28 post-MCAo, IL-4 EVs were able to increase the density of GFP$^+$ cells in the ischemic penumbra when compared to animals receiving either i-EVs or vehicle alone (Fig 5A, B). The amount of GFP$^+$ OPCs co-expressing the early differentiation marker NG2 did not differ among all the experimental conditions (Fig 5C, D), while the percentages of GFP$^+$ cells co-expressing GPR17 (indicative of a pre-oligodendrocyte stage) or the mature myelinating oligodendrocyte marker GSTπ were significantly increased after IL-4 EVs infusion compared to vehicle or i-EVs conditions (Fig 5E-H). Furthermore, the administration of IL-4 EVs resulted in a significant increase of FluoroMyelin stain in the ipsilateral corpus callosum of ischemic mice (Fig 5I, J), indicating that efficient myelin repair occurred. These results suggest that the infusion of microglial IL-4 EVs at late stages after MCAo was able to promote a selective response to ischemic damage of the pool of OPCs expressing GPR17 and to foster their terminal maturation, contributing to enhanced remyelination.

Infusion of pro-regenerative microglia-derived EVs fosters functional recovery of ischemic mice

The most invalidating consequences of cerebral ischemia are the long-lasting persistence of cognitive and motor disability in patients.[41,42] However, a reliable analysis of these deficits is difficult to be implemented in ischemic mice, due to the extremely high rate of spontaneous recovery and to compensatory mechanisms involving the intact contralateral hemisphere which occur within the first week after ischemia, thus making long-term evaluations very challenging.[43] In this respect, one important feature of stroke-induced deficit is commonly referred to as "*neglect"* and consists in the inability to perceive stimuli coming from the region contralateral to the ischemic hemisphere, with important consequences for spatial cognition and explorative behaviors.[44] Of note, such defect is maintained in rodent models of cerebral ischemia, manifesting as a turning preference toward the ipsilateral side, with a consequent reduction in the percentage of contralateral turns.[43]

To evaluate the impact of IL-4 EVs on the turning preference of ischemic mice, a Y-maze test[45] was performed at day 14 post-MCAo, before minipump implantation, and at day 28 post-MCAo, after IL-4 EVs or vehicle infusion (Fig 6A, B). As expected, at day 14 post-MCAo, ischemic animals displayed a significative reduction in the percentage of contralateral turns as compared to sham-operated controls (Fig 6C). No significant differences in locomotor activity and spontaneous alternation were detected at day 14 post-MCAo between ischemic mice and sham-operated controls (Fig 6D, E). Interestingly, at day 28 post-MCAo, vehicle-treated animals still maintained a significant impairment of contralateral turns, while in mice receiving IL-4 EVs a reversion of turning preference was observed, which restored functionality up to that observed in sham-operated controls (Fig 6F). Also at this time point, no changes in locomotor activity and spontaneous alternation among the three experimental groups were recorded (Fig 6G, H).

In addition, at day 28 post-MCAo, infusion of IL-4 EVs resulted in a significant reduction of the percentage of ischemia-induced neuronal tissue loss, mainly affecting the motor cortex, as compared to vehicle-treated mice (Fig 6I-L), possibly contributing to the functional amelioration observed.

Transmembrane tumor necrosis factor-α (tm**TNF) is involved in the beneficial effects exerted by microglial EVs on OPC maturation**

To explore the direct effects of IL-4 EVs on the pool of GFP^+ cells, OPCs were isolated from GPR17-iCreER^{T2}:CAG-eGFP mice and exposed *in vitro* to either IL-4 EVs or medium alone (CTRL) for 72 hours.

Notably, after *in vitro* exposure to 4-hydroxytamoxifen (OH-TAM), no significant differences were detected in the percentage of GFP^+ cells between CTRL and IL-4 EVs-treated cultures (Fig 7A, B). Immunofluorescence analysis showed that IL-4 EVs significantly increased the percentage of mature MBP^+ cells compared to CTRL (Fig 7A-C), demonstrating a direct pro-differentiating effect of IL-4 EVs. Moreover, the fraction of GFP^+ cells co-expressing MBP was significantly higher in cultures exposed to IL-4 EVs with respect to CTRL, while no significant changes were observed in the GFP negative pool of progenitors (Fig 7D). This suggests that the subpopulation of GFP^+ OPCs, namely the GPR17-expressing pool of cells,[12] is indeed more prone to differentiate and more responsive to the pro-differentiating action of microglial EVs. Accordingly, in both CTRL and IL-4 EVs conditions, the percentage of MBP^+ cells was significantly higher in the GFP^+ OPC subset as compared to the GFP negative one (Fig 7D).

Recent evidence indicates that TNFα is increased in EVs derived from activated microglia[46] and macrophages.[47] In particular, EVs derived from these myeloid cells

are enriched in the transmembrane form (tmTNF) of the cytokine,[47] which promotes oligodendrocyte differentiation and remyelination both *in vitro* and *in vivo* via activation of TNFR2 receptor,[48] suggesting that TNFα may play a role in the pro-differentiating effects of IL-4 EVs. To address this issue, primary OPCs were exposed to IL-4 EVs in the presence of the selective soluble TNFα (solTNF) inhibitor XPro^{TM}1595 (XPro) or the non-selective solTNF and tmTNF blocker etanercept (ETN). Interestingly, while XPro did not inhibit the increase in the percentage of MBP$^+$ cells induced by IL-4 EVs, ETN counteracted the pro-differentiating action of IL-4 EVs (Fig 7E, F). These data provide concrete clues of a possible involvement of tmTNF/TNFR2 axis in the mechanism underlying the beneficial effect of microglial EVs on OPC maturation.

Discussion

Despite representing only a subset of all Olig2$^+$ oligodendrocyte lineage cells,[12] the subpopulation of OPCs expressing the GPR17 receptor (indicated as GFP$^+$ cells in this study) has attracted great interest for its capacity to rapidly respond to injury and trigger reparative mechanisms after cerebral ischemia[14] or upon other neurodegenerative conditions.[15,16] However, the spontaneous differentiation capability of this pool of progenitors is often counteracted by local inflammation, which makes their pro-myelinating attempts ineffective.[14–16] Our previous data have suggested the importance of locally released factors in addressing the reparative function of the GPR17-expressing cells, but the type of cells and mechanisms at the basis of this *in situ* regulation were unclear. Here, we uncover the pivotal role of the crosstalk between microglia/macrophages and GPR17-expressing OPCs in shaping brain repair and functional recovery after ischemic stroke.

We demonstrate that Iba1$^+$ immune cells exert a beneficial action on the pool of GPR17-expressing OPCs in the early injury phase, while their pro-resolving properties are lost at late disease stages. The change in Iba1$^+$ effector cell function is clearly reflected by morphological alterations, with microglia/macrophages acquiring a hypertrophic and ameboid shape in the early post ischemic phase and then becoming dystrophic at late stages. Furthermore, we show that EVs collected from microglia cultured with a pro-regenerative stimulus are able to both counteract the late ineffective phenotype of resident immune cells and foster the differentiation of GPR17-expressing OPCs to mature functional cells, leading to increased neurological recovery. By *in vitro* experiments, we provide evidence for a direct beneficial effect exerted by microglial EVs on the pool of GPR17-expressing OPCs and highlight EV-carried tmTNF as a putative pivotal player in mediating microglia-to-OPC communication.

Early after ischemia, microglia/macrophages enhance OPCs density and limit myelin damage

Though it is known that neuroinflammation mediated by peripherally derived macrophages and their CNS resident counterpart microglia greatly influences neuronal network activity in the ischemic injured brain,[21,49] its exact impact on oligodendrocytes during the acute and chronic phases after ischemic stroke still remains unclear. This is a key point to be addressed, considering the importance of myelin repair in neurological recovery[11] and the potential of immune cells (particularly microglia) in supporting myelin regeneration in different neurological disorders, such as multiple sclerosis.[50,51]

By immunohistochemistry for phenotypic markers and pharmacological immune cell

depletion, we show that Iba1$^+$ cells are rapidly activated after stroke, with a persistent response evolving over time. At early stages after stroke, pro-inflammatory and pro-regenerative Iba1$^+$ cells coexist and are committed to a protective function, with a large fraction of cells co-expressing both inflammatory and pro-resolving markers. The presence of this mixed phenotype is in agreement with recent evidence displacing the canonical dichotomous classification of microglia activation in favour of a higher diversity of functional states,[52] and may help to explain the lack of selectivity of $GdCl_3$ treatment (which was previously shown to specifically target pro-inflammatory cells[23,37]) observed at early stage after ischemia. On the contrary, at late phases of the disease, the pro-inflammatory component gradually dominates the site of injury. This is in line with previous observations by other groups.[22,53,54] Specifically, the activation of local microglia was suggested to precede and dominate over the infiltration of peripheral macrophages during the first days post-stroke, when they assume a protective phenotype,[18] having them a limited capacity to acquire a pro-inflammatory state.[55] Conversely, blood-derived macrophages were reported to contribute to delayed post-ischemic inflammation and injury,[56,57] as their depletion reduces brain atrophy volume and neurological deficits 14 days after transient ischemia.[58] However, infiltrating macrophages were also shown to be essential for maintaining a pro-regenerative anti-inflammatory polarization of Iba1$^+$ immune cells early after ischemic brain injury, therefore contributing to the endogenous protective events at this early time point.[22,35] Although our study did not discriminate between microglia and blood-borne macrophages, results from our depletion experiments highlight a novel protective action of both immune cells early after ischemia, namely, to sustain the rapid reaction of GPR17-expressing OPCs at the lesion site,[14] and to limit myelin damage. Indeed, early after $GdCl_3$-mediated immune cell depletion, the number of

GFP^+ OPCs was significantly reduced, in line with a role for microglia/macrophages in promoting OPC proliferation,[23] as also supported by our data showing a reduced percentage of GFP^+ OPCs incorporating BrdU in $GdCl_3$-treated mice. However, since previous results also demonstrated a positive impact of immune cells on OPC migration,[27] it can't be completely excluded that a lack of chemoattractive molecules released by microglia/macrophages might contribute to the impaired recruitment of GFP^+ cells observed. The reduction of both myelin thickness and myelinated axon density observed in $GdCl_3$-treated animals further indicated the critical contribution of these immune cells in preserving myelin integrity at early times after ischemia.

At late stages after ischemic injury, $Iba1^+$ immune cells lose their pro-regenerative capacity

In addition to the data above, we show that, at later stages after MCAo, depletion of pro-inflammatory $Iba1^+$ immune cells was paralleled by an increase in GFP^+ OPC density, suggesting that chronicization of the pro-inflammatory response of $Iba1^+$ cells potentiates damage progression at delayed times after ischemic injury.[18,59] Despite this effect, no improvement of oligodendroglial differentiation was detected in these conditions, indicating that the remaining microglial/macrophagic cells did not retain their ability to efficiently sustain OPC maturation. In line with this consideration, at later stages after ischemia, $Iba1^+$ cell morphology appeared to be dystrophic, resembling that of senescent cells during physiological aging or chronic neurodegenerative conditions.[32] Dystrophic morphology has been supposed to be induced by microglia/macrophage overstimulation and has been frequently associated with impaired capacity of the cells to exert pro-regenerative and neuroprotective functions.[32] Hence, to promote structural and functional recovery at late stages after

stroke, therapeutic approaches should be aimed at selectively restoring microglia/macrophage regenerative effector functions rather than simply depleting these myeloid cells, which inevitably leads to the loss of their beneficial effects.

An EV-based strategy to prevent immune cell detrimental function and foster differentiation of GPR17-expressing OPCs

Among the strategies able to redirect microglia/macrophages toward beneficial functions,[60] microglial EVs recently emerged as a promising approach able to modulate the phenotype of recipient myeloid cells in experimental models of neurological disorder.[28,39,40] Consistently, here we showed that microglial EVs are able to induce significant modifications in recipient $Iba1^+$ cells in the ischemic penumbra, with different responses depending on the activation state of donor cells as previously demonstrated.[30,40,61] Importantly, EVs derived from pro-regenerative microglia were able to restore the pro-resolving activities of recipient microglia/macrophages at late stages after ischemia, thus contributing to create the permissive local environment required for efficient repair processes, including oligodendroglial maturation and remyelination.[16,51] This is in line with our recent evidence that EVs collected from pro-regenerative microglia have the capacity, when infused *in vivo,* to enhance the endogenous reparative response of OPCs at focal myelin lesions.[27] The present study significantly extends these findings, by demonstrating that IL-4 EVs specifically stimulate the response of GPR17-expressing OPCs at ischemic injury borders and markedly rescued neurological deficits in ischemic mice.

Several issues remain to be explored, including how EVs are taken up by recipient cells,[62] and what are the molecular mechanisms by which they exert their pro-

differentiating effects on OPCs. Intriguingly, our data suggest that TNFα, previously shown to be enriched in EVs derived from activated microglia[27,46] may, at least in part, contribute to the pro-differentiating effects of IL-4 EVs by activating oligodendroglial TNFR2.[48,63] This is in line with very recent results showing that release of TNFα by microglia in response to demyelinating injury is essential to start myelin repair processes.[64] Nevertheless, the lipid cargo of microglial EVs was also demonstrated to enhance OPC differentiation,[27] suggesting that a combination of factors, rather than a single molecule, might be responsible for EV-mediated beneficial effects.

Taken together, the data presented in this study advance our understanding of the complex interaction between microglia/macrophages and OPCs after stroke and pave the way for developing EV-based strategies[65] aimed at implementing myelin repair and tissue recovery after stroke.

Materials and methods

Animals and experimental procedures

The procedures concerning animal care, surgery, and sacrifice were performed in accordance with national (D.L. n.26, 2014) and International laws and policies (EU Directive 2010/63/EU) and approved and authorized by the National Ministry of Health-University of Milan Committee (approval number 868/2016-PR). Moreover, all protocols used were in accordance with ARRIVE guidelines. GPR17-iCreER^{T2}:CAG-eGFP reporter mice[14] have been used, bred and housed at the animal facility of the Department of Pharmacological and Biomolecular Sciences in Milan. After genotyping, performed on DNA extracts from tail clippings as described,[12] eleven weeks old double transgenic GPR17-iCreER^{T2}:CAG-eGFP mice received 10

mg tamoxifen (Sigma-Aldrich, Taufkirchen, Germany), dissolved in 10% ethanol and 90% corn oil, three times by gavage once every second day to induce recombination. After 3 weeks of wash-out, mice were anesthetized with ketamine (80 mg/kg) and xylazine (16 mg/kg) and underwent permanent Middle Cerebral Artery occlusion (MCAo) as previously described.[14,66] Briefly, a vertical midline skin incision was made between the right orbit and ear. The temporal muscle was excised, the oblique edge of a drill bit was used to thin an approximately 1 mm circle of bone overlying the MCA. The thinned bone and the dura mater were incised with a 29-gauge needle tip and the right MCA was exposed and permanently occluded by means of microbipolar coagulation (SAMED MB122) just proximal to the origin of the olfactory branch. Sham-operated mice underwent the same surgical procedures with exception of artery occlusion. The retracted temporalis muscle was allowed to fall back into place and sutured. The animals were then allowed to recover from anesthesia. Male and female mice have been equally employed in all the experiments. The mortality rate we observed in MCAo procedure was 10%. For microglia characterization, mice were sacrificed at days 1, 3, 7 and 14 post-MCAo (n =3 mice for each time point), while for microglia/macrophage depletion and EVs infusion experiments mice were sacrificed at days 17, 28 and 42 post-MCAo (n =4–9 mice for each time point; see details below).

Depletion of microglia/macrophage cell populations

To achieve microglia/macrophages depletion, we chose a strategy based on the administration of gadolinium chloride ($GdCl_3$).[23,37] Briefly, GPR17-iCreER^{T2}:CAG-eGFP mice received daily intranasal doses of $GdCl_3$ (10 mg/kg/day; Sigma-Aldrich, Taufkirchen, Germany), dissolved in water added with 40% PEG300, or vehicle. A

first group of mice has been treated starting from 2 hours before MCAo until day 3 after the surgery (early depletion). A second group of mice received $GdCl_3$ from day 14 to day 17 post-MCAo (late depletion). Both groups were sacrificed immediately at the end of the treatment. Finally, a third group of animals has been exposed to the late depletion protocol and sacrificed at day 42 (n=5 mice per experimental condition). To evaluate GFP^+ OPCs proliferation, animals included in the early depletion experiments also received daily intraperitoneal injections of the DNA synthesis marker 5-bromo-2'-deoxyuridine (BrdU; Sigma-Aldrich, Taufkirchen, Germany) dissolved in saline (50 mg/kg/day) starting from 4 hours after MCAo until sacrifice.

Primary microglia cultures

Mixed glial cell cultures, containing both astrocytes and microglia, were established from C57/Bl6 wild-type mice (P2) (Charles River, Lecco, Italy) and maintained for 10 days in the presence of South American fetal bovine serum (Life Technologies, Monza, Italy) that optimizes microglia expansion. Microglia were harvested by orbital shaking for 40 min at 1300 r.p.m. and re-plated on poly-l-ornithine-coated tissue culture dishes (50 μg/ml, Sigma-Aldrich, Taufkirchen, Germany). To minimize the activation, pure microglia (> 98%)[26] were kept for 24 hours in low-serum (1%) medium. Cells were then stimulated with a cocktail of Th1 cytokines, i.e. 20 ng/ml IL-1β (Peprotech, Milan, Italy), 20 ng/ml TNF-α (Peprotech, Milan, Italy) and 25 ng/ml IFN-ɣ (Sigma-Aldrich, Taufkirchen, Germany), or with 20 ng/ml IL-4 (R&D, Milan, Italy) for 48 hours. At the end of treatment, microglia were washed and stimulated with ATP to increase EVs production, as described.[26] Primary murine microglia were maintained in the absence of stimuli (NS), under inflammatory (i-MG) or pro-regenerative (IL-4 MG) conditions for 48 hours. Real-time PCR have been

performed as follows to check the expression of pro-inflammatory and pro-regenerative markers (Fig S6).

RNA isolation and quantification

After ATP stimulation, cell supernatant was collected for EV isolation (see below) and donor cells were lysed with TRIZOL® reagent (Life Technologies, Monza, Italy). Total RNA was extracted using Direct-zol™ RNA Micro-Prep (Zymo Research, Irvine, CA, USA) according to the manufacturer's instructions. RNA was then pre-treated with RQ1 DNase (Promega, Milan, Italy) for eliminating genomic DNA contamination. Retrotranscription of 400 ng RNA was performed with SensiFAST™ cDNA synthesis kit (Bioline, London, UK). For real-time PCR, several mixes were prepared according to the number of interested genes. Each mix included Master Mix 2x (Life Techonologies, Monza, Italy), 250 nM probe (Arg1 Mm00475988_m1; Ym1 Mm00657889_mH; IL-1β Mm00434228_m1; TNFα Mm00443258_m1; iNOS Mm00440502_m1; Rpl13a Mm05910660_g1; Life Technologies, Monza, Italy) and 20 ng of cDNA. Gene-expression was analyzed with TaqMan® Gene Expression Assay and normalized to housekeeping gene Rpl13a expression using CFX96 real-time PCR system (BioRad Laboratories, Segrate, Italy) following the manufacturer's protocol. Data are presented as mean of $\log_2$(fold change) ± SE.

Isolation and quantification of microglia-derived EVs

To isolate EVs, polarized microglia were stimulated with 1 mM ATP for 30 min in KRH (125 mM NaCl, 5 mM KCl, 1.2 mM MgSO4, 1.2 mM KH2PO, 2 mM CaCl2, 6 mM d-glucose, and 25 mM HEPES/NaOH, pH 7.4). The culture supernatant was collected and EVs were pelleted at 100.000 g after pre-clearing from cells and debris

at 300 g, as previously described.[67] EV pellets were resuspended and used immediately after isolation. EV size and concentration were measured by Tunable Resistive Pulse Sensing (TRPS) technique, using an Izon qNano instrument (Izon, Christchurch, New Zealand). EVs produced by 1×10^6 microglia in 1 hour were re-suspended in a volume of 100 µl. A reagent kit from Izon (Izon EV reagent kit) was used for both pre-treating the pore and suspending EVs in order to prevent EV binding to the pore or spontaneous EV aggregation. NP300 nanopore (Izon, Christchurch, New Zealand) was employed and CPC200 (carboxylated polystyrene particles, supplied by Izon and diluted following manufacturer's instructions) were used as standards. In each experiment, the same applied voltage, pressure and pore stretch values were set for all sample and calibration particle recordings. Data acquisition and analysis were performed using Izon Control Suite software (version V3.3).

EV intracerebral infusion

At day 14 post-MCAo, mice received infusion of IL-4 EVs (n=9), i-EVs (n=4) or vehicle (n=9). Briefly, approximately 2×10^8 EVs, produced by 1.5×10^6 microglia and dissolved in 150 µl of sterile saline, were infused in the ipsilateral *corpus callosum* of ischemic mice (coordinates from bregma: 1.0 mm rostral, 1.0 mm lateral, 2 mm deep) using osmotic mini-pumps (1007D equipped with Brain Infusion kit 3, Alzet, Cupertino, CA, USA) over 7 days at 0.5 µl/h delivery rate. To limit EV degradation, minipumps were filled with freshly isolated EVs and implanted within a few hours. Using this method, stability of microglial EVs into the minipumps has been reported for more than 4 days and the presence of injected GFP-labelled EVs within the tissue, as well as their interaction with both microglia and OPCs at the

injury site, has been previously demonstrated.[27] Vehicle-treated animals were obtained with delivery of saline solution alone. Mice were sacrificed at day 28 post-MCAo.

Behavioral assessment

To evaluate persistent asymmetries in mice turning preference before and after infusion of IL-4 EVs, the Y-maze test was performed.[45] Briefly, animals have been positioned in the middle of a Y-shaped maze, consisting of three plastic arms at 120° angle from each other, and left free to explore for 8 minutes, during which the number and sequence of entries in each arm have been manually recorded by an operator blinded to the experimental groups. It has been considered an entry when all four limbs were within the new arm, and one spontaneous alternation has been counted when the animal entered all three different arms consecutively. *Locomotor activity* (total number of entries in a new arm), % *alternation* (# of spontaneous alternations/# of total triads*100) and *% of contralateral turns* (# of contralateral turns when entering a new arm/# of total turns*100) have been calculated. First, stroke-induced alterations have been assessed on ischemic mice (MCAo; n=14) at day 14 post-MCAo, before EV administration. As controls, sham-operated mice (n=5), undergoing the same surgical procedures of MCAo mice with exception of artery occlusion, have been utilized. Immediately after this first behavioral evaluation, MCAo animals have been randomly assigned using the RAND.BETWEEN function of Excel (Microsoft, Redmond, WA, USA) to infusion of IL-4 EVs (n=7) or vehicle (n=7) as described above. ANOVA followed by Helmert contrast analysis excluded any bias in the assignment of MCAo mice to vehicle or IL-4 EVs group ($p>0.05$). At day 28 post-MCAo, the Y-maze test has been repeated to evaluate the impact of IL-4

EV infusion on mice turning preference with respect to both vehicle-treated animals and sham-operated controls.

Immunohistochemical (IHC) analysis

At the day of the sacrifice, after anesthesia with ketamine (80 mg/kg) and xylazine (16 mg/kg), mice were perfused with 0.01 M phosphate buffered-saline (PBS) and then 4% paraformaldehyde in 0.01 M PBS for at least 25 min. Brains were removed, post-fixed 1 hour in the same solution and then cryoprotected in 30% sucrose solution until precipitation at 4 °C. Coronal sections of 20 μm thickness have been collected using a microtome and incubated with the following primary antibodies: chicken anti-GFP (1:1400; Aves Labs, Inc., Tigard, OR, USA); rat anti-BrdU (1:200; Abcam, Cambridge, UK); rat anti-CD68 (1:400; BioRad Laboratories, Segrate, Italy); rat anti-CD16/CD32 (1:200; BD Biosciences, Milan, Italy); rabbit anti-GSTπ (1:500; MBL, Woburn, MA, USA), rabbit anti-Iba1 (1:30000; Wako, Japan); rabbit anti-NeuN (1:100; Cell Signaling Technologies, Danvers, MA, USA); rabbit anti-NG2 (1:2000; Millipore, Milan, Italy), rabbit anti-GFAP (1:500; Dako, Glostrup, Denmark), rabbit anti-GPR17 (1:2500; custom antibody produced by Primm, Milan, Italy)[68] and rabbit anti-Ym1 (1:100; Stemcell Technologies, Cambridge, UK). Incubation with primary antibodies was made overnight at 4 °C in 0.01 M PBS with 1% normal goat serum (Dako, Glostrup, Denmark) and 0.3% Triton-X 100. The sections were exposed for 2 hours at room temperature to the corresponding secondary antibodies (all goat) conjugated with Alexa Fluor 488, 555 or 633 (1:600; Life Technologies, Monza, Italy). For rabbit anti-NG2, GPR17 and Iba1, the signal intensity was enhanced using the High Sensitivity Tyramide Signal Amplification kit (Perkin-Elmer, Monza, Italy) following the manufacturer's instructions. For double GFP/BrdU labeling, staining of

BrdU was performed last, after fixing sections with 4% paraformaldehyde for 10 min and incubating them with HCl 2M for 45 min at 37 °C. Nuclei were labeled with Hoechst 33258 (0.06 μg/ml; Life Technologies, Monza, Italy). For myelin staining, FluoroMyelin^{TM} Red stain (1:300; Life Technologies, Monza, Italy) has been used following manufacturer's instructions. For the quantitative analysis, the peri-infarct region (0-500 μm from the boundary of the ischemic lesion), and its corresponding area in the contralateral hemisphere, have been considered. Images were acquired at ×20 magnification (647.04 x 647.04 μm) using a confocal microscope (merge of 6-μm z-stack at 2-μm intervals; A1R, Nikon, Tokyo, Japan). Iba1 staining was performed using 633 fluorophore, and the false color green has been applied in representative images to better display co-localization with other markers in red. To visualize brain damage, hematoxylin-eosin (HE; Sigma-Aldrich, Taufkirchen, Germany) staining has been performed and images acquired by means of a slide scanner (NanoZoomer S60, Hamamatsu Photonics, Hamamatsu City, Japan). The number of GFP-positive, double positive GFP&NG2, GFP&GPR17, GFP&GSTπ, GFP&BrdU, Iba1&CD16/32, Iba1&Ym1, Iba1&CD68, triple positive Iba1&CD16/32&Ym1, the densitometric analysis of GFAP and FluoroMyelin staining and the area of $NeuN^+$ and HE-stained tissue were manually quantified by a blinded investigator, using the software Fiji/ImageJ, on three slices per mouse taken from −1.00 to 0.00 mm from bregma. For analysis of tissue loss, the area of NeuN or HE staining has been manually measured for each slice both in the ipsilateral hemisphere and in the intact contralateral one and the percentage of tissue loss has been calculated as *% tissue loss = (area contra – area ipsi)/area contra * 100.*

Morphological analysis of microglia/macrophages

Analysis of microglia/macrophage cell morphology was carried out on 20 µm-thick brain sections stained for Iba1.[69] For characterization, images were acquired at ischemic injury borders at day 3 and day 14 post-MCAo and in the corresponding region of the contralateral hemisphere at day 3 post-MCAo. To evaluate the impact of EVs infusion on $Iba1^+$ cell morphology, images were acquired at day 28 post-MCAo at lesion boundaries in animals treated with IL-4 EVs, i-EVs or vehicle. Analysis was carried out by exploiting the semi-automatic Matlab-based tool 3DMorph.[70] 130-150 cells from 3-4 animals for each experimental condition have been analyzed. Among morphological parameters considered were *number of branchpoints* and *ramification index*, calculated as *cell surface area/(4π × ((3 × cell volume)/(4π))2/3* and gaining score 1 for round-shaped cells and higher values as cell ramification increases, both reflecting the complexity of cell branching. Moreover, we analyzed *cell volume*, which gives indications about the intensity of cell activation, and *cell territory*, which is proportional to cell volume and to the number and the length of cell processes and is indicative of the brain area surveilled by each individual cell.

Transmission Electron Microscopy (TEM)

To perform TEM analysis, mice receiving early intranasal administration of $GdCl_3$ or vehicle (n=3) were trans-cardially perfused with 2% paraformaldehyde, 2.5% glutaraldehyde in 0.15 M sodium cacodylate buffer (pH 7.4; Sigma-Aldrich, Taufkirchen, Germany). Then, tissues were post-fixed for additional 24hours at 4°C and processed as described.[71] Briefly, coronal sections of 100-µm thickness were collected using a vibratome and selected areas of the ipsilateral corpus callosum adjacent to the ischemic damage, together with the corresponding regions of the contralateral hemisphere, were manually dissected using a stereoscope. Samples were

post-fixed in 2% osmium tetroxide, stained using 1% uranyl acetate for 45 min, dehydrated and embedded in Spurr's epoxy resin baked at 60°C for 48h. Finally, thin sections (70 nm) were cut using a Leica EM UC6 ultramicrotome (Leica Microsystems, Wetzlar, Germany), stained with a saturated solution of uranyl acetate in 20% ethanol and 1% lead citrate and grids were observed using a Philips CM10 TEM (FEI, Eindhoven, Netherland). For quantitative analysis, images at x13500 magnification were taken and *g-ratio, myelin thickness, axon diameter* and *myelinated axon density* were calculated on 300 axons for each experimental condition using the software Fiji/ImageJ as described.[27]

Primary OPC cultures

Primary OPCs were isolated from total brain of GPR17-iCreER^{T2}:CAG-eGFP mice at post-natal day 2 (P2). Briefly, brains were dissected from pups and maintained at 4°C in Tissue Storage Solution® (Miltenyi Biotec, Bologna, Italy) for 3 hours during genotyping (performed on tail biopsies as described above). Only brains deriving from double transgenic GPR17-iCreER^{T2}:CAG-eGFP mice were pulled together and dissociated into single cell suspensions using Papain-based Neural Tissue Dissociation Kit (Miltenyi Biotec, Bologna, Italy). Then, PDGFRα^{+} OPCs were sorted by MACS separation after incubation with anti-PDGFRα magnetic microbeads (Miltenyi Biotec, Bologna, Italy) following the manufacturer's instructions. PDGFRα^{+} cells (approximately 250.000 cells obtained from each pup) have been cultured on poly-DL-ornithine (Sigma-Aldrich, Taufkirchen, Germany) coated 24-well plates (30.000 cells/well) in OPC proliferation medium containing Neurobasal (Life Technologies, Monza, Italy), 2% B27 (Life Technologies, Monza, Italy), 1% L-glutamine (Euroclone, Pero, Italy), 1% penicillin/streptomycin (Euroclone, Pero,

Italy), 10 ng/ml PDGF-AA (Sigma-Aldrich, Taufkirchen, Germany), 10 ng/ml FGF2 (Space Import Export, Milan, Italy) and 1μM 4-Hydroxitamoxifen (to induce GFP expression; Sigma-Aldrich, Taufkirchen, Germany). After 2 days, cells were switched to differentiation medium containing DMEM (Euroclone, Pero, Italy), 1% N-2 supplement (Life Technologies, Monza, Italy), 2% B27, 0.01% BSA (Sigma-Aldrich, Taufkirchen, Germany), 1% L-glutamine, 1% penicillin/streptomycin and 10 ng/ml T3 (Sigma-Aldrich, Taufkirchen, Germany) and 4 hours later, medium alone (CTRL) or IL-4 EVs were added to OPC culture (1:2 OPC-microglia ratio) in presence or absence of the non-selective TNFα inhibitor Etanercept (ETN) (200 ng/ml; Wyeth, Madison, NJ, USA) or XPro^{TM}1595 (200 ng/ml; Xencor, Monrovia, CA, USA), a selective solTNF inhibitor.[72] Cells have been differentiated for 3 days and then fixed at room temperature with 4% paraformaldehyde (Sigma-Aldrich, Taufkirchen, Germany) in 0.01 M PBS containing 0.12 M sucrose (Sigma-Aldrich, Taufkirchen, Germany) for immunocytochemistry. Under these culture conditions, contaminating astrocytes and microglia were routinely less than 1% each. To evaluate $GdCl_3$ toxicity *in vitro*, primary OPCs have been cultured in proliferating conditions in presence of $GdCl_3$ concentrations demonstrated to be toxic for microglial cultures, i.e. 270 μM and 1 mM,[73] or vehicle alone (CTRL) for 72 hours. Cells were then fixed as described above and processed for immunocytochemistry.

Immunocytochemistry

Labelling was performed incubating cells overnight at 4°C with the following primary antibodies diluted in Goat Serum Dilution Buffer [GSDB: 450 mM NaCl (Sigma-Aldrich, Taufkirchen, Germany), 20 mM sodium phosphate buffer pH 7.4, 15% goat serum (Life Technologies, Monza, Italy), 0.3% Triton X-100 (Sigma-Aldrich,

Taufkirchen, Germany)]: rat anti-MBP (1:200; Millipore, Milan, Italy), chicken anti-GFP (1:1400; Aves Labs, Inc., Tigard, OR, USA). Cells were then incubated for 1 hour at room temperature with the following secondary antibodies: goat anti-rat conjugated to Alexa Fluor 555, goat anti-chicken conjugated to Alexa Fluor 488 (1:600 in GSDB; Life Technologies, Monza, Italy). In $GdCl_3$-treated cultures, OPC viability has been assessed by incubating cells for 15 minutes at room temperature with propidium iodide (PI; 1 μg/ml; Sigma-Aldrich, Taufkirchen, Germany). Nuclei were labelled with Hoechst33258 (0.3 μg/ml; Life Technologies, Monza, Italy). Coverslips were finally mounted with a fluorescent mounting medium (Dako, Glostrup, Denmark) and analyzed using an inverted fluorescence microscope (200M; Zeiss, Jena, Germany) connected to a PC equipped with the Axiovision software (Zeiss, Jena, Germany). For cell counts, 30 fields were acquired at x20 magnification (0.07 mm^2/field; three coverslips for each experimental condition deriving from three independent experiments). Analysis was performed using the Fiji/ImageJ software.

Statistical analysis

For each experimental procedure, the proper sample size has been calculated by mean of the G*Power 3.1 software,[74] estimating effect size and standard deviation based on previously published data[14,23,27,45] and fixing the alpha value (type 1 error) at the level of 5% (p=0.05) and the power at 80%.

Data are expressed as mean ± standard error (SE). Statistical analysis was performed using the Prism 7 software (GraphPad, San Diego, CA, USA). Gaussian distribution of the values in each experimental group has been assessed using Shapiro-Wilk (for n<8) or D'Agostino-Pearson (for n>8) normality tests. For all comparisons between two groups with a normal distribution, unpaired Student's t-test was performed, while

for groups without normal distribution nonparametric Mann-Whitney test was used. For multiple comparison testing, depending on the experimental design, one-way or two-way analysis of variance (ANOVA) accompanied by Tukey's post-hoc test was used for groups with normal distribution, whereas nonparametric Kruskal-Wallis test followed by Dunn's post-hoc analysis was performed when normal distribution of the values could not be assumed. For correlation analysis, two-tailed Pearson test was used. Differences were considered significant for p-value <0.05.

Data availability

Further information and data that support the findings of this study are available from the corresponding author upon reasonable request.

Author contributions

MF conceived and supervised the project. SR, PG, MPA, CV and MF designed experiments. SR, PG, EB, LC, ML carried out experiments, data acquisition and analysis. MC performed brain ischemic surgery. SR, PG, LS, MPA, CV and MF contributed to data interpretation and discussion. SR and MF wrote the original draft. All co-authors critically revised and edited the manuscript.

Acknowledgements

We are grateful to Prof. Roberta Brambilla (University of Miami, Miami, FL, USA) for fruitful discussion and Dr. David E.Szymkowski (Xencor, Inc., Monrovia, CA, USA) for providing XPro^{TM}1595. We thank Prof. Flavia Antonucci (University of Milan, Milan, Italy) for help with Y-maze apparatus, Dr. Norma Lattuada (University of Milan, Milan, Italy) for technical support with electron microscopy analysis and

Dr. Martina Gabrielli (CNR, Institute of Neuroscience, Milan, Italy) for assistance with characterization of EVs. Part of this work was carried out at NOLIMITS, an advanced imaging facility established by Università degli Studi di Milano. This study was supported by Fondazione Cariplo, Italy (grant n.2015-0910 to MF), by Università degli Studi di Milano (Piano di Sostegno alla Ricerca, 2015-2017 to MF), and by Italian Ministry of University and Research-MIUR project "Dipartimenti di Eccellenza 2018-2022" to Dept. of Pharmacological and Biomolecular Sciences.

Conflict of interest

The authors declare that they have no conflict of interest.

References

1. Benjamin, EJ, Muntner, P, Alonso, A, Bittencourt, MS, Callaway, CW, Carson, AP, *et al.* (2019). *Heart Disease and Stroke Statistics-2019 Update: A Report From the American Heart Association*. *Circulation* **139**, 56–528pp.
2. Zhao, L-R and Willing, A (2018). Enhancing endogenous capacity to repair a stroke-damaged brain: An evolving field for stroke research. *Progresss Neurobiol.* **163**–**164**: 5–26.
3. Rost, NS, Cougo, P, Lorenzano, S, Li, H, Cloonan, L, Bouts, MJRJ, *et al.* (2018). Diffuse microvascular dysfunction and loss of white matter integrity predict poor outcomes in patients with acute ischemic stroke. *J. Cereb. Blood Flow Metab.* **38**: 75–86.
4. Marshall, RS (2015). Progress in intravenous thrombolytic therapy for acute stroke. *JAMA Neurol.* **72**: 928–934.
5. Duncan, ID, Brower, A, Kondo, Y, Curlee, JF and Schultz, RD (2009).

Extensive remyelination of the CNS leads to functional recovery. *Proc. Natl. Acad. Sci. U. S. A.* **106**: 6832–6836.

6. Zhang, R, Chopp, M and Zhang, ZG (2013). Oligodendrogenesis after cerebral ischemia. *Front. Cell. Neurosci.* **7**: 201.
7. Han, L, Cai, W, Mao, L, Liu, J, Li, P, Leak, RK, *et al.* (2015). Rosiglitazone Promotes White Matter Integrity and Long-Term Functional Recovery after Focal Cerebral Ischemia. *Stroke* **46**: 2628–2636.
8. Gelosa, P, Bonfanti, E, Castiglioni, L, Delgado-Garcia, JM, Gruart, A, Fontana, L, *et al.* (2019). Improvement of fiber connectivity and functional recovery after stroke by montelukast, an available and safe anti-asthmatic drug. *Pharmacol. Res.* **142**: 223–236.
9. Kremer, D, Göttle, P, Hartung, H-P and Küry, P (2016). Pushing Forward: Remyelination as the New Frontier in CNS Diseases. *Trends Neurosci.* **39**: 246–263.
10. Crawford, AH, Tripathi, RB, Richardson, WD and Franklin, RJM (2016). Developmental Origin of Oligodendrocyte Lineage Cells Determines Response to Demyelination and Susceptibility to Age-Associated Functional Decline. *Cell Rep.* **15**: 761–773.
11. Franklin, RJM and Ffrench-Constant, C (2017). Regenerating CNS myelin - From mechanisms to experimental medicines. *Nat. Rev. Neurosci.* **18**: 753–769.
12. Viganò, F, Schneider, S, Cimino, M, Bonfanti, E, Gelosa, P, Sironi, L, *et al.* (2016). GPR17 expressing NG2-Glia: Oligodendrocyte progenitors serving as a reserve pool after injury. *Glia* **64**: 287–299.
13. Fumagalli, M, Daniele, S, Lecca, D, Lee, PR, Parravicini, C, Douglas Fields,

R, *et al.* (2011). Phenotypic changes, signaling pathway, and functional correlates of GPR17-expressing neural precursor cells during oligodendrocyte differentiation. *J. Biol. Chem.* **286**: 10593–10604.

14. Bonfanti, E, Gelosa, P, Fumagalli, M, Dimou, L, Viganò, F, Tremoli, E, *et al.* (2017). The role of oligodendrocyte precursor cells expressing the GPR17 receptor in brain remodeling after stroke. *Cell Death Dis.* **8**: e2871.
15. Coppolino, GT, Marangon, D, Negri, C, Menichetti, G, Fumagalli, M, Gelosa, P, *et al.* (2018). Differential local tissue permissiveness influences the final fate of GPR17-expressing oligodendrocyte precursors in two distinct models of demyelination. *Glia* **66**: 1118–1130.
16. Lecca, D, Raffaele, S, Abbracchio, MP and Fumagalli, M (2020). Regulation and signaling of the GPR17 receptor in oligodendroglial cells. *Glia* **2**: 1–11.
17. Iadecola, C and Anrather, J (2011). The immunology of stroke: From mechanisms to translation. *Nat. Med.* **17**: 796–808.
18. Hu, X, Li, P, Guo, Y, Wang, H, Leak, RK, Chen, S, *et al.* (2012). Microglia/macrophage polarization dynamics reveal novel mechanism of injury expansion after focal cerebral ischemia. *Stroke* **43**: 3063–3070.
19. Jin, WN, Shi, SXY, Li, Z, Li, M, Wood, K, Gonzales, RJ, *et al.* (2017). Depletion of microglia exacerbates postischemic inflammation and brain injury. *J. Cereb. Blood Flow Metab.* **37**: 2224–2236.
20. Otxoa-de-Amezaga, A, Miró-Mur, F, Pedragosa, J, Gallizioli, M, Justicia, C, Gaja-Capdevila, N, *et al.* (2019). Microglial cell loss after ischemic stroke favors brain neutrophil accumulation. *Acta Neuropathol.* **137**: 321–341.
21. Szalay, G, Martinecz, B, Lénárt, N, Környei, Z, Orsolits, B, Judák, L, *et al.* (2016). Microglia protect against brain injury and their selective elimination

dysregulates neuronal network activity after stroke. *Nat. Commun.* **7**.

22. Rajan, WD, Wojtas, B, Gielniewski, B, Gieryng, A, Zawadzka, M and Kaminska, B (2019). Dissecting functional phenotypes of microglia and macrophages in the rat brain after transient cerebral ischemia. *Glia* **67**: 232–245.

23. Miron, VE, Boyd, A, Zhao, JW, Yuen, TJ, Ruckh, JM, Shadrach, JL, *et al.* (2013). M2 microglia and macrophages drive oligodendrocyte differentiation during CNS remyelination. *Nat. Neurosci.* **16**: 1211–1218.

24. Behrendt, G, Baer, K, Buffo, A, Curtis, MA, Faull, RL, Rees, MI, *et al.* (2013). Dynamic changes in myelin aberrations and oligodendrocyte generation in chronic amyloidosis in mice and men. *Glia* **61**: 273–286.

25. Budnik, V, Ruiz-Cañada, C and Wendler, F (2016). Extracellular vesicles round off communication in the nervous system. *Nat. Rev. Neurosci.* **17**: 160–172.

26. Prada, I, Gabrielli, M, Turola, E, Iorio, A, D'Arrigo, G, Parolisi, R, *et al.* (2018). Glia-to-neuron transfer of miRNAs via extracellular vesicles: a new mechanism underlying inflammation-induced synaptic alterations. *Acta Neuropathol.* **135**: 529–550.

27. Lombardi, M, Parolisi, R, Scaroni, F, Bonfanti, E, Gualerzi, A, Gabrielli, M, *et al.* (2019). Detrimental and protective action of microglial extracellular vesicles on myelin lesions: astrocyte involvement in remyelination failure. *Acta Neuropathol.* **138**: 987–1012.

28. Verderio, C, Muzio, L, Turola, E, Bergami, A, Novellino, L, Ruffini, F, *et al.* (2012). Myeloid microvesicles are a marker and therapeutic target for neuroinflammation. *Ann. Neurol.* **72**: 610–624.

29. Joshi, P, Turola, E, Ruiz, A, Bergami, A, Libera, DD, Benussi, L, *et al.* (2014). Microglia convert aggregated amyloid-β into neurotoxic forms through the shedding of microvesicles. *Cell Death Differ.* **21**: 582–593.

30. Nigro, A, Colombo, F, Casella, G, Finardi, A, Verderio, C and Furlan, R (2016). Myeloid Extracellular Vesicles: Messengers from the Demented Brain. *Front. Immunol.* **7**: 1.

31. Drago, F, Lombardi, M, Prada, I, Gabrielli, M, Joshi, P, Cojoc, D, *et al.* (2017). ATP Modifies the Proteome of Extracellular Vesicles Released by Microglia and Influences Their Action on Astrocytes. *Front. Pharmacol.* **8**: 910.

32. Savage, JC, Carrier, M and Tremblay, MÈ (2019). Morphology of Microglia Across Contexts of Health and Disease. *Methods Mol. Biol.* **2034**, Humana Press Inc.: pp 13–26.

33. Ransohoff, RM and Perry, VH (2009). Microglial Physiology: Unique Stimuli, Specialized Responses. *Annu. Rev. Immunol.* **27**: 119–145.

34. Colonna, M and Butovsky, O (2017). Microglia Function in the Central Nervous System During Health and Neurodegeneration. *Annu. Rev. Immunol.* **35**: 441–468.

35. Perego, C, Fumagalli, S, Zanier, ER, Carlino, E, Panini, N, Erba, E, *et al.* (2016). Macrophages are essential for maintaining a M2 protective response early after ischemic brain injury. *Neurobiol. Dis.* **96**: 284–293.

36. Villa, A, Gelosa, P, Castiglioni, L, Cimino, M, Rizzi, N, Pepe, G, *et al.* (2018). Sex-Specific Features of Microglia from Adult Mice. *Cell Rep.* **23**: 3501–3511.

37. Van Steenwinckel, J, Schang, A-L, Krishnan, ML, Degos, V, Delahaye-Duriez, A, Bokobza, C, *et al.* (2019). Decreased microglial Wnt/b-catenin signalling drives microglial pro-inflammatory activation in the developing brain. *Brain*

142: 3806–3833.

38. Wylot, Mieczkowski, Niedziolka, Kaminska and Zawadzka (2019). Csf1 Deficiency Dysregulates Glial Responses to Demyelination and Disturbs CNS White Matter Remyelination. *Cells* **9**: 99.

39. Casella, G, Colombo, F, Finardi, A, Descamps, H, Ill-Raga, G, Spinelli, A, *et al.* (2018). Extracellular Vesicles Containing IL-4 Modulate Neuroinflammation in a Mouse Model of Multiple Sclerosis. *Mol. Ther.* **26**: 2107–2118.

40. Grimaldi, A, Serpe, C, Chece, G, Nigro, V, Sarra, A, Ruzicka, B, *et al.* (2019). Microglia-Derived Microvesicles Affect Microglia Phenotype in Glioma. *Front. Cell. Neurosci.* **13**: 41.

41. Stinear, C (2010). Prediction of recovery of motor function after stroke. *Lancet Neurol.* **9**: 1228–1232.

42. Stinear, CM (2017). Prediction of motor recovery after stroke: advances in biomarkers. *Lancet Neurol.* **16**: 826–836.

43. Balkaya, MG, Trueman, RC, Boltze, J, Corbett, D and Jolkkonen, J (2018). Behavioral outcome measures to improve experimental stroke research. *Behav. Brain Res.* **352**: 161–171.

44. Vallar, G and Calzolari, E (2018). Unilateral spatial neglect after posterior parietal damage. *Handb. Clin. Neurol.* **151**, Elsevier B.V.: pp 287–312.

45. Saadoun, S, Waters, P, Bell, BA, Vincent, A, Verkman, AS and Papadopoulos, MC (2010). Intra-cerebral injection of neuromyelitis optica immunoglobulin G and human complement produces neuromyelitis optica lesions in mice. *Brain* **133**: 349–361.

46. Yang, Y, Boza-Serrano, A, Dunning, CJR, Clausen, BH, Lambertsen, KL and

Deierborg, T (2018). Inflammation leads to distinct populations of extracellular vesicles from microglia. *J. Neuroinflammation* **15**: 1–19.

47. Soni, S, O'Dea, KP, Tan, YY, Cho, K, Abe, E, Romano, R, *et al.* (2019). ATP redirects cytokine trafficking and promotes novel membrane TNF signaling via microvesicles. *FASEB J.* **33**: 6442–6455.
48. Madsen, PM, Motti, D, Karmally, S, Szymkowski, DE, Lambertsen, KL, Bethea, JR, *et al.* (2016). Oligodendroglial TNFR2 mediates membrane TNF-dependent repair in experimental autoimmune encephalomyelitis by promoting oligodendrocyte differentiation and remyelination. *J. Neurosci.* **36**: 5128–5143.
49. Kronenberg, G, Uhlemann, R, Richter, N, Klempin, F, Wegner, S, Staerck, L, *et al.* (2018). Distinguishing features of microglia- and monocyte-derived macrophages after stroke. *Acta Neuropathol.* **135**: 551–568.
50. Davies, CL and Miron, VE (2018). Distinct origins, gene expression and function of microglia and monocyte-derived macrophages in CNS myelin injury and regeneration. *Clin. Immunol.* **189**: 57–62.
51. Lloyd, AF and Miron, VE (2019). The pro-remyelination properties of microglia in the central nervous system. *Nat. Rev. Neurol.*: 29–34doi:10.1038/s41582-019-0184-2.
52. Stratoulias, V, Venero, JL, Tremblay, M and Joseph, B (2019). Microglial subtypes: diversity within the microglial community. *EMBO J.* **38**.
53. Perego, C, Fumagalli, S and De Simoni, MG (2011). Temporal pattern of expression and colocalization of microglia/macrophage phenotype markers following brain ischemic injury in mice. *J. Neuroinflammation* **8**.
54. Peruzzotti-Jametti, L, Donegá, M, Giusto, E, Mallucci, G, Marchetti, B and Pluchino, S (2014). The role of the immune system in central nervous system

plasticity after acute injury. *Neuroscience* **283**: 210–221.

55. Durafourt, BA, Moore, CS, Zammit, DA, Johnson, TA, Zaguia, F, Guiot, MC, *et al.* (2012). Comparison of polarization properties of human adult microglia and blood-derived macrophages. *Glia* **60**: 717–727.

56. Dimitrijevic, OB, Stamatovic, SM, Keep, RF and Andjelkovic, A V. (2007). Absence of the chemokine receptor CCR2 protects against cerebral ischemia/reperfusion injury in mice. *Stroke* **38**: 1345–1353.

57. Breckwoldt, MO, Chen, JW, Stangenberg, L, Aikawa, E, Rodriguez, E, Qiu, S, *et al.* (2008). Tracking the inflammatory response in stroke in vivo by sensing the enzyme myeloperoxidase. *Proc. Natl. Acad. Sci. U. S. A.* **105**: 18584–18589.

58. Ma, Y, Li, Y, Jiang, L, Wang, L, Jiang, Z, Wang, Y, *et al.* (2016). Macrophage depletion reduced brain injury following middle cerebral artery occlusion in mice. *J. Neuroinflammation* **13**: 38.

59. An, C, Shi, Y, Li, P, Hu, X, Gan, Y, Stetler, RA, *et al.* (2014). Molecular dialogs between the ischemic brain and the peripheral immune system: Dualistic roles in injury and repair. *Prog. Neurobiol.* **115**: 6–24.

60. Fumagalli, M, Lombardi, M, Gressens, P and Verderio, C (2018). How to reprogram microglia toward beneficial functions. *Glia* **66**: 2531–2549.

61. Garzetti, L, Menon, R, Finardi, A, Bergami, A, Sica, A, Martino, G, *et al.* (2014). Activated macrophages release microvesicles containing polarized M1 or M2 mRNAs. *J. Leukoc. Biol.* **95**: 817–825.

62. Van Niel, G, D'Angelo, G and Raposo, G (2018). Shedding light on the cell biology of extracellular vesicles. *Nat. Rev. Mol. Cell Biol.* **19**: 213–228.

63. Raffaele, S, Lombardi, M, Verderio, C and Fumagalli, M (2020). TNF

Production and Release from Microglia via Extracellular Vesicles: Impact on Brain Functions. *Cells* **9**: 2145.

64. Cunha, MI, Su, M, Cantuti-Castelvetri, L, Müller, SA, Schifferer, M, Djannatian, M, *et al.* (2020). Pro-inflammatory activation following demyelination is required for myelin clearance and oligodendrogenesis. *J. Exp. Med.* **217**.

65. El Andaloussi, S, Mäger, I, Breakefield, XO and Wood, MJA (2013). Extracellular vesicles: Biology and emerging therapeutic opportunities. *Nat. Rev. Drug Discov.* **12**: 347–357.

66. Storini, C, Bergamaschini, L, Gesuete, R, Rossi, E, Maiocchi, D and De Simoni, MG (2006). Selective inhibition of plasma kallikrein protects brain from reperfusion injury. *J. Pharmacol. Exp. Ther.* **318**: 849–854.

67. Gabrielli, M, Battista, N, Riganti, L, Prada, I, Antonucci, F, Cantone, L, *et al.* (2015). Active endocannabinoids are secreted on extracellular membrane vesicles. *EMBO Rep.* **16**: 213–220.

68. Bonfanti, E, Bonifacino, T, Raffaele, S, Milanese, M, Morgante, E, Bonanno, G, *et al.* (2020). Abnormal Upregulation of GPR17 Receptor Contributes to Oligodendrocyte Dysfunction in SOD1 G93A Mice. *Int. J. Mol. Sci.* **21**: 2395.

69. Magni, G, Boccazzi, M, Bodini, A, Abbracchio, MP, van den Maagdenberg, AM and Ceruti, S (2019). Basal astrocyte and microglia activation in the central nervous system of Familial Hemiplegic Migraine Type I mice. *Cephalalgia* **39**: 1809–1817.

70. York, EM, Ledue, JM, Bernier, LP and Macvicar, BA (2018). 3dmorph automatic analysis of microglial morphology in three dimensions from ex vivo and in vivo imaging. *eNeuro* **5**.

71. Murru, L, Vezzoli, E, Longatti, A, Ponzoni, L, Falqui, A, Folci, A, *et al.* (2017). Pharmacological Modulation of AMPAR Rescues Intellectual Disability-Like Phenotype in Tm4sf2-/y Mice. *Cereb. Cortex* **27**: 5369–5384.

72. Karamita, M, Barnum, C, Möbius, W, Tansey, MG, Szymkowski, DE, Lassmann, H, *et al.* (2017). Therapeutic inhibition of soluble brain TNF promotes remyelination by increasing myelin phagocytosis by microglia. *JCI insight* **2**.

73. Mizgerd, JP, Molina, RM, Stearns, RC, Brain, JD and Warner, AE (1996). Gadolinium induces macrophage apoptosis. *J. Leukoc. Biol.* **59**: 189–195.

74. Charan, J and Kantharia, N (2013). How to calculate sample size in animal studies? *J. Pharmacol. Pharmacother.* **4**: 303–306.

Figure Legends

Figure 1 - Microglia/macrophage activation at the boundary of ischemic lesion increases over time after MCAo.

A Schematic representation of the experimental protocol exploited to study microglial activation following MCAo.

B Representative images of $Iba1^+$ cells at the boundary of ischemic lesion (0-500 µm) at day 1, 3, 7 and 14 after MCAo and in the corresponding region of the contralateral hemisphere at day 1 post-MCAo. Scale bar: 50 µm. Magnifications show ischemia-induced modifications of $Iba1^+$ cell morphology. Scale bar: 25 µm.

C Representative images of $CD16/32^+$ cells at the boundary of ischemic lesion (0-500 µm) at day 1, 3, 7 and 14 after MCAo and in the corresponding region of the contralateral hemisphere at day 1 post-MCAo. Scale bar: 50 µm.

D Representative images of $Ym1^+$ cells at the boundary of ischemic lesion (0-500

µm) at day 1, 3, 7 and 14 after MCAo and in the corresponding region of the contralateral hemisphere at day 1 post-MCAo. Scale bar: 50 µm.

E Quantification of the density of $Iba1^+$ cells in the boundary of ischemic lesion (0-500 µm) and in the corresponding region of the contralateral hemisphere at day 1, 3, 7 and 14 after MCAo (n=3). Data are expressed as mean ± SE. Two-way ANOVA (Interaction $p<0.0001$, Time $p<0.0001$, MCAo $p<0.0001$) followed by Tukey's post-hoc analysis (p values relative to multiple comparisons are reported in the tables).

F Quantification of the density of $Iba1^+$ cells co-expressing the pro-inflammatory marker CD16/32 at the boundary of ischemic lesion (0-500 µm) and in the corresponding region of the contralateral hemisphere at day 1, 3, 7 and 14 after MCAo (n=3). Data are expressed as mean ± SE. Two-way ANOVA (Interaction $p<0.0001$, Time $p<0.0001$, MCAo $p<0.0001$) followed by Tukey's post-hoc analysis (p values relative to multiple comparisons are reported in the tables).

G Quantification of the density of $Iba1^+$ cells co-expressing the pro-regenerative marker Ym1 at the boundary of ischemic lesion (0-500 µm) and in the corresponding region of the contralateral hemisphere at day 1, 3, 7 and 14 after MCAo (n=3). Data are expressed as mean ± SE. Two-way ANOVA (Interaction $p=0.0967$, Time $p=0.2763$, MCAo $p<0.0001$) followed by Tukey's post-hoc analysis (p values relative to multiple comparisons are reported in the tables).

Figure 2 - Partial depletion of microglia/macrophages in the early phase after MCAo impairs GPR17-expressing OPC response and exacerbates myelin damage.

A Schematic representation of the experimental protocol exploited for early depletion of microglia/macrophages after MCAo.

B Representative images of cells stained for Iba1, CD16/32, Ym1, GFP and GFP/BrdU at the boundary of ischemic lesion (0-500 µm) at day 3 post-MCAo following intranasal administration of $GdCl_3$ or vehicle. Arrowheads indicate cells double positive for GFP and BrdU. Scale bar: 50 µm.

C Quantification of the density of total $Iba1^+$, $Iba1^+$&$CD16/32^+$ and $Iba1^+$&$Ym1^+$ cells at the boundary of ischemic lesion (0-500 µm) at day 3 post-MCAo following intranasal administration of $GdCl_3$ or vehicle (n=4). Data are expressed as mean ± SE. Student's t test.

D Quantification of the density of GFP^+ OPCs and of the percentage of GFP^+ cells incorporating BrdU at the boundary of ischemic lesion (0-500 µm) at day 3 post-MCAo following intranasal administration of $GdCl_3$ or vehicle (n=4). Data are expressed as mean ± SE. Student's t test.

E Scatter plot representation of the linear correlation between the densities of $Iba1^+$ cells (x axis) and GFP^+ OPCs (y axis) at the boundary of ischemic lesion (0-500 µm) at day 3 post-MCAo. Green dots correspond to $GdCl_3$-treated animals, while blue dots represent vehicle-treated animals. For correlation analysis, two-tailed Pearson test was used.

F Representative electron micrographs showing myelinated axons in the ipsilateral corpus callosum of ischemic mice at day 3 post-MCAo following intranasal administration of $GdCl_3$ or vehicle and in the corresponding region of the contralateral hemisphere of vehicle-treated animals. Scale bar: 1 µm.

G Quantification of g-ratio, myelin thickness, axon diameter and myelinated axon density in the ipsilateral corpus callosum of ischemic mice at day 3 post-MCAo following intranasal administration of $GdCl_3$ or vehicle and in the corresponding region of the contralateral hemisphere of vehicle-treated animals (n=3; 300

fibers/experimental condition have been analyzed). Data are expressed as mean ± SE. One-way ANOVA followed by Tukey's post-hoc analysis.

Figure 3 - Partial depletion of microglia/macrophages at the late stage after MCAo promotes GPR17-expressing OPC response but has no impact on their maturation.

A Schematic representation of the experimental protocol exploited for late depletion of microglia/macrophages after MCAo.

B Representative images of cells stained for Iba1, CD16/32, Ym1 and GFP at the boundary of ischemic lesion (0-500 µm) at day 17 post-MCAo following intranasal administration of $GdCl_3$ or vehicle. Scale bar: 50 µm.

C Quantification of the density of total $Iba1^+$, $Iba1^+$&$CD16/32^+$ and $Iba1^+$&$Ym1^+$ cells at the boundary of ischemic lesion (0-500 µm) at day 17 post-MCAo following intranasal administration of $GdCl_3$ or vehicle (n=5). Data are expressed as mean ± SE. Student's t test.

D Quantification of the density of GFP^+ OPCs at the boundary of ischemic lesion (0-500 µm) at day 17 post-MCAo following intranasal administration of $GdCl_3$ or vehicle (n=6). Data are expressed as mean ± SE. Student's t test.

E Scatter plot representation of the linear correlation between the densities of $Iba1^+$ cells (x axis) and GFP^+ OPCs (y axis) at the boundary of ischemic lesion (0-500 µm) at day 17 post-MCAo. Green dots correspond to $GdCl_3$-treated animals, while blue dots represent vehicle-treated animals. For correlation analysis, two-tailed Pearson test was used.

F Representative images of cells stained for GFP and GSTπ at the boundary of ischemic lesion (0-500 µm) at day 42 post-MCAo following intranasal administration

of $GdCl_3$ or vehicle. Scale bar: 50 µm. Magnifications show cells co-expressing GFP and GSTπ. Scale bar: 25 µm.

G Quantification of the density of total GFP^+ OPCs and GFP^+&$GST\pi^+$ cells at the boundary of ischemic lesion (0-500 µm) at day 42 post-MCAo following intranasal administration of $GdCl_3$ or vehicle (n=5-6). Data are expressed as mean ± SE. Student's t test.

H Representative images of myelin visualized using FluoroMyelin Red stain in the corpus callosum (CC, delimited by white dashed lines) at the boundary of ischemic lesion (0-500 µm) at day 42 post-MCAo, following intranasal administration of $GdCl_3$ or vehicle. Scale bar: 50 µm.

I Quantification of the percentage of $FluoroMyelin^+$ area in the corpus callosum at the boundary of ischemic lesion (0-500 µm) at day 42 post-MCAo, following intranasal administration of $GdCl_3$ or vehicle (n=5-6). Data are expressed as mean ± SE and normalized to vehicle set to 100.

Figure 4 - Infusion of pro-regenerative microglia-derived EVs at late stages after ischemia promotes a beneficial polarization of microglia/macrophages.

A Schematic representation of the experimental protocol exploited for the infusion of microglia-derived EVs after MCAo.

B Representative images of cells stained for Iba1 and CD16/32 at the boundary of ischemic lesion (0-500 µm) at day 28 post-MCAo, following infusion of i-EVs, IL-4 EVs or vehicle. Scale bar: 50 µm.

C Representative images of cells stained for Iba1 and Ym1 at the boundary of ischemic lesion (0-500 µm) at day 28 post-MCAo, following infusion of i-EVs, IL-4 EVs or vehicle. Scale bar: 50 µm.

D Quantification of the density of total $Iba1^+$, $Iba1^+$&$CD16/32^+$ and $Iba1^+$&$Ym1^+$ cells at the boundary of ischemic lesion (0-500 µm) at day 28 post-MCAo, following infusion of i-EVs, IL-4 EVs or vehicle (n=4). Data are expressed as mean ± SE. One-way ANOVA followed by Tukey's post-hoc analysis.

E Quantification of $Iba1^+$ microglia/macrophage number of branchpoints, ramification index, cell volume and cell territory at the boundary of ischemic lesion (0-500 µm) at day 28 post-MCAo, following infusion of i-EVs, IL-4 EVs or vehicle (130-150 cells from 3-4 animals/experimental condition have been analyzed). Data are expressed as mean ± SE. Kruskal-Wallis test followed by Dunn's post-hoc analysis.

Figure 5 - Infusion of pro-regenerative microglia-derived EVs at late stages after ischemia enhances GPR17-expressing OPC differentiation.

A Representative images of GFP^+ OPCs at the boundary of ischemic lesion (0-500 µm) at day 28 post-MCAo, following infusion of i-EVs, IL-4 EVs or vehicle. Scale bar: 50 µm.

B Quantification of the density of GFP^+ OPCs at the boundary of ischemic lesion (0-500 µm) at day 28 post-MCAo, following infusion of i-EVs, IL-4 EVs or vehicle (n=4-9). Data are expressed as mean ± SE. One-way ANOVA followed by Tukey's post-hoc analysis.

C Representative images of cells stained for GFP and NG2 at the boundary of ischemic lesion (0-500 µm) at day 28 post-MCAo, following infusion of i-EVs, IL-4 EVs or vehicle. Scale bar: 50 µm. Magnifications show cells co-expressing GFP and NG2. Scale bar: 25 µm.

D Quantification of the percentage of GFP^+ OPCs co-expressing NG2 at the boundary of ischemic lesion (0-500 µm) at day 28 post-MCAo, following infusion of i-EVs, IL-

4 EVs or vehicle (n=4-9). Data are expressed as mean ± SE.

E Representative images of cells stained for GFP and GPR17 at the boundary of ischemic lesion (0-500 µm) at day 28 post-MCAo, following infusion of i-EVs, IL-4 EVs or vehicle. Scale bar: 50 µm. Magnifications show cells co-expressing GFP and GPR17. Scale bar: 25 µm.

F Quantification of the percentage of GFP^+ OPCs co-expressing GPR17 at the boundary of ischemic lesion (0-500 µm) at day 28 post-MCAo, following infusion of i-EVs, IL-4 EVs or vehicle (n=3-4). Data are expressed as mean ± SE. One-way ANOVA followed by Tukey's post-hoc analysis.

G Representative images of cells stained for GFP and GSTπ at the boundary of ischemic lesion (0-500 µm) at day 28 post-MCAo, following infusion of i-EVs, IL-4 EVs or vehicle. Scale bar: 50 µm. Magnifications show cells co-expressing GFP and GSTπ. Scale bar: 25 µm.

H Quantification of the percentage of GFP^+ OPCs co-expressing GSTπ at the boundary of ischemic lesion (0-500 µm) at day 28 post-MCAo, following infusion of i-EVs, IL-4 EVs or vehicle (n=4-9). Data are expressed as mean ± SE. One-way ANOVA followed by Tukey's post-hoc analysis.

I Representative images of myelin visualized using FluoroMyelin Red stain in the corpus callosum (CC, delimited by white dashed lines) at the boundary of ischemic lesion (0-500 µm) at day 28 post-MCAo, following infusion of i-EVs, IL-4 EVs or vehicle. Scale bar: 50 µm.

J Quantification of the percentage of $FluoroMyelin^+$ area in the corpus callosum at the boundary of ischemic lesion (0-500 µm) at day 28 post-MCAo, following infusion of i-EVs, IL-4 EVs or vehicle (n=4). Data are expressed as mean ± SE and normalized to vehicle set to 100. One-way ANOVA followed by Tukey's post-hoc analysis.

Figure 6 - Infusion of pro-regenerative microglia-derived EVs at late stages after ischemia promotes functional recovery of ischemic mice.

A Schematic representation of the experimental protocol exploited for behavioral analysis before and after the infusion of microglia-derived EVs after MCAo.

B Schematic representation of the Y-maze test to evaluate the turning preference of ischemic mice.

C Quantification of the percentage of contralateral turns made in the Y-maze test at day 14 post-MCAo by MCAo mice (n=14) and sham-operated controls (n=5). Data are expressed as mean ± SE. Student's t-test.

D Quantification of the locomotor activity of MCAo mice (n=14) and sham-operated controls (n=5) during the Y-maze test at day 14 post-MCAo. Data are expressed as mean ± SE.

E Quantification of the percentage of spontaneous alternations made in the Y-maze test at day 14 post-MCAo by MCAo mice (n=14) and sham-operated controls (n=5). Data are expressed as mean ± SE.

F Quantification of the percentage of contralateral turns made in the Y-maze test at day 28 post-MCAo by sham-operated controls (n=5) and MCAo mice after infusion of IL-4 EVs (n=7) or vehicle (n=7). Data are expressed as mean ± SE. One-way ANOVA followed by Tukey's post-hoc analysis.

G Quantification of the locomotor activity of sham-operated controls (n=5) and MCAo mice after infusion of IL-4 EVs (n=7) or vehicle (n=7) during the Y-maze test at day 28 post-MCAo. Data are expressed as mean ± SE.

H Quantification of the percentage of spontaneous alternations made in the Y-maze test at day 28 post-MCAo by sham-operated controls (n=5) and MCAo mice after

infusion of IL-4 EVs (n=7) or vehicle (n=7). Data are expressed as mean ± SE.

I Representative images of $NeuN^+$ tissue at day 28 post-MCAo, following infusion of IL-4 EVs or vehicle. Green dashed lines delineate the area of NeuN staining in the ipsilateral hemisphere. White dashed lines correspond to the projection of $NeuN^+$ area in the intact contralateral hemisphere. Scale bar: 1 mm.

J Representative images of the ischemic region in hematoxylin-eosin (HE) stained sections at day 28 post-MCAo, following infusion of IL-4 EVs or vehicle. Black dashed lines delineate the ischemic core. Scale bar: 400 µm.

K Quantification of the percentage of $NeuN^+$ tissue loss at day 28 post-MCAo after infusion of IL-4 EVs or vehicle (n=5). Data are expressed as mean ± SE. Student's t-test.

L Quantification of the percentage of HE-labeled tissue loss at day 28 post-MCAo after infusion of IL-4 EVs or vehicle (n=5). Data are expressed as mean ± SE. Student's t-test.

Figure 7 - Direct effects of microglial IL-4 EVs on GFP^+ OPC maturation *in vitro*.

A Representative images showing cells expressing GFP and MBP in primary OPC cultures from GPR17-iCreER^{T2}:CAG-eGFP mice exposed to IL-4 EVs or medium alone (CTRL). Scale bar: 50 µm.

B Quantification of the percentage of GFP^+ cells in primary OPC cultures from GPR17-iCreER^{T2}:CAG-eGFP mice exposed to IL-4 EVs or CTRL. Data are expressed as mean ± SE (n=9 coverslips from 3 independent experiments).

C Quantification of the total percentage of MBP^+ cells in primary OPC cultures from GPR17-iCreER^{T2}:CAG-eGFP mice exposed to IL-4 EVs or CTRL. Data are

expressed as mean ± SE (n=9 coverslips from 3 independent experiments). Student's t-test.

D Quantification of the percentage of GFP^+ and GFP^{neg} cells co-expressing MBP in primary OPC cultures from GPR17-iCreER^{T2}:CAG-eGFP mice exposed to IL-4 EVs or CTRL. Data are expressed as mean ± SE (n=9 coverslips from 3 independent experiments). One-way ANOVA followed by Tukey's post-hoc analysis.

E Representative images showing MBP^+ cells in primary OPC cultures exposed to IL-4 EVs or CTRL in presence or absence of the selective solTNF inhibitor XPro^{TM}1595 (XPro) and of the non-selective TNFα inhibitor etanercept (ETN). Scale bar: 50 μm.

F Quantification of the total percentage of MBP^+ cells in primary OPC cultures exposed to IL-4 EVs or CTRL in presence or absence of XPro or ETN. Data are expressed as mean ± SE (n=9 coverslips from 3 independent experiments). One-way ANOVA followed by Tukey's post-hoc analysis.

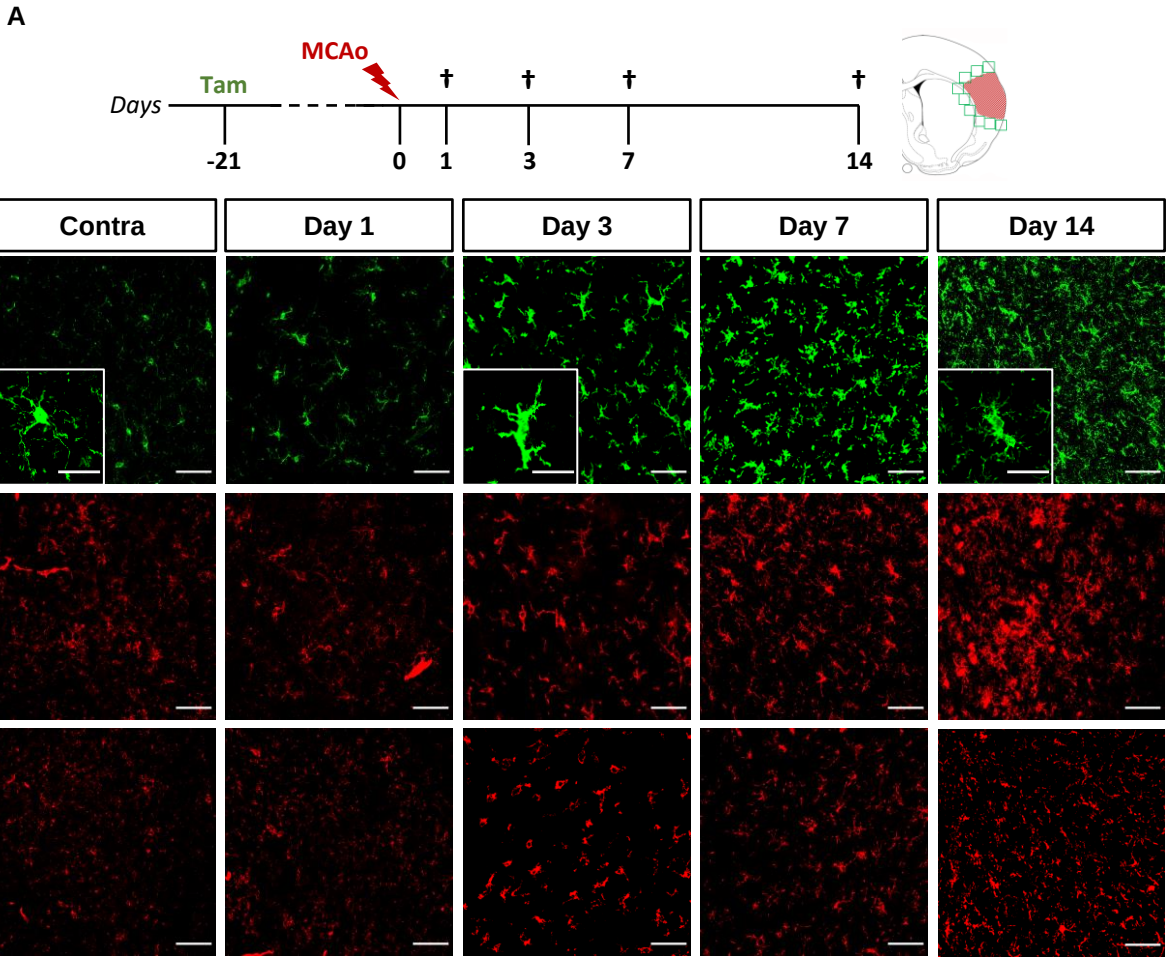

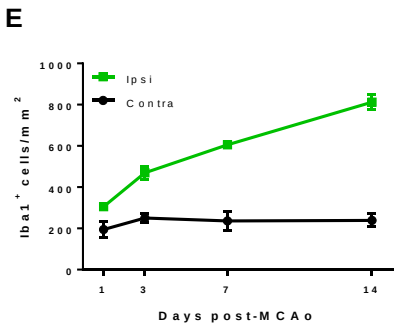

Ipsi vs Contra	p value
Day 1	ns
Day 3	0.0007
Day 7	<0.0001
Day 14	<0.0001

Days (ipsi)	p value
1 vs 3	0.0106
1 vs 7	<0.0001
1 vs 14	<0.0001
3 vs 7	0.0368
3 vs 14	<0.0001
7 vs 14	0.0016

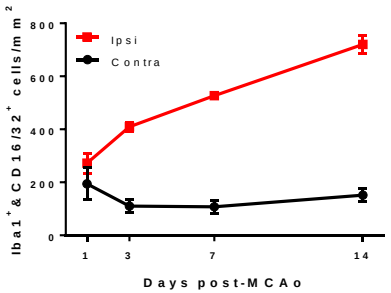

Ipsi vs Contra	p value
Day 1	ns
Day 3	<0.0001
Day 7	<0.0001
Day 14	<0.0001

Days (ipsi)	p value
1 vs 3	0.0431
1 vs 7	0.0003
1 vs 14	<0.0001
3 vs 7	ns
3 vs 14	<0.0001
7 vs 14	0.0037

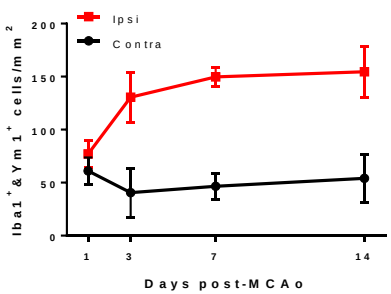

Ipsi vs Contra	p value
Day 1	ns
Day 3	0.0133
Day 7	0.0047
Day 14	0.0057

Days (ipsi)	p value
1 vs 3	ns
1 vs 7	0.0590
1 vs 14	0.0413
3 vs 7	ns
3 vs 14	ns
7 vs 14	ns

Raffaele S et al., 2020_Figure 1

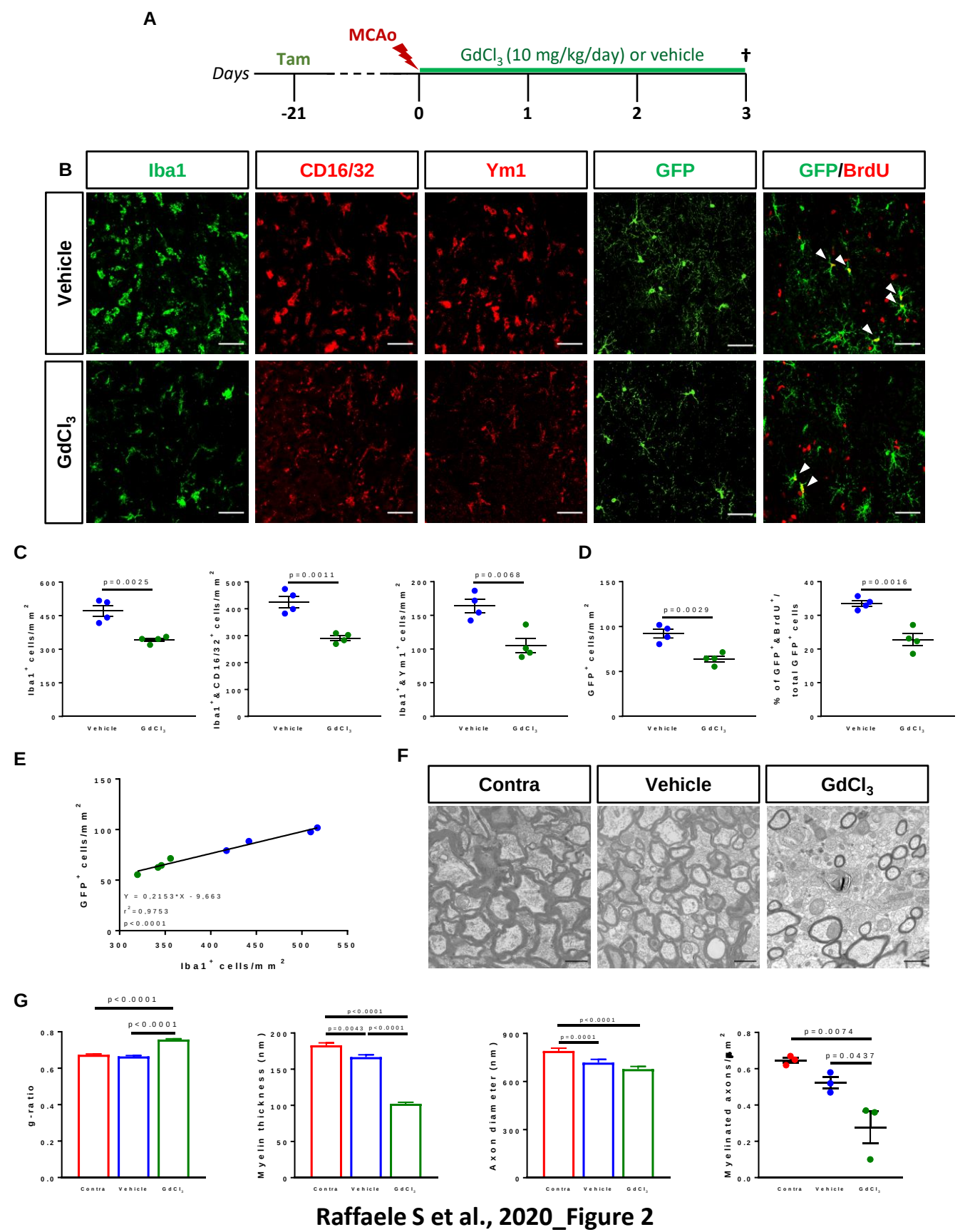

Raffaele S et al., 2020_Figure 2

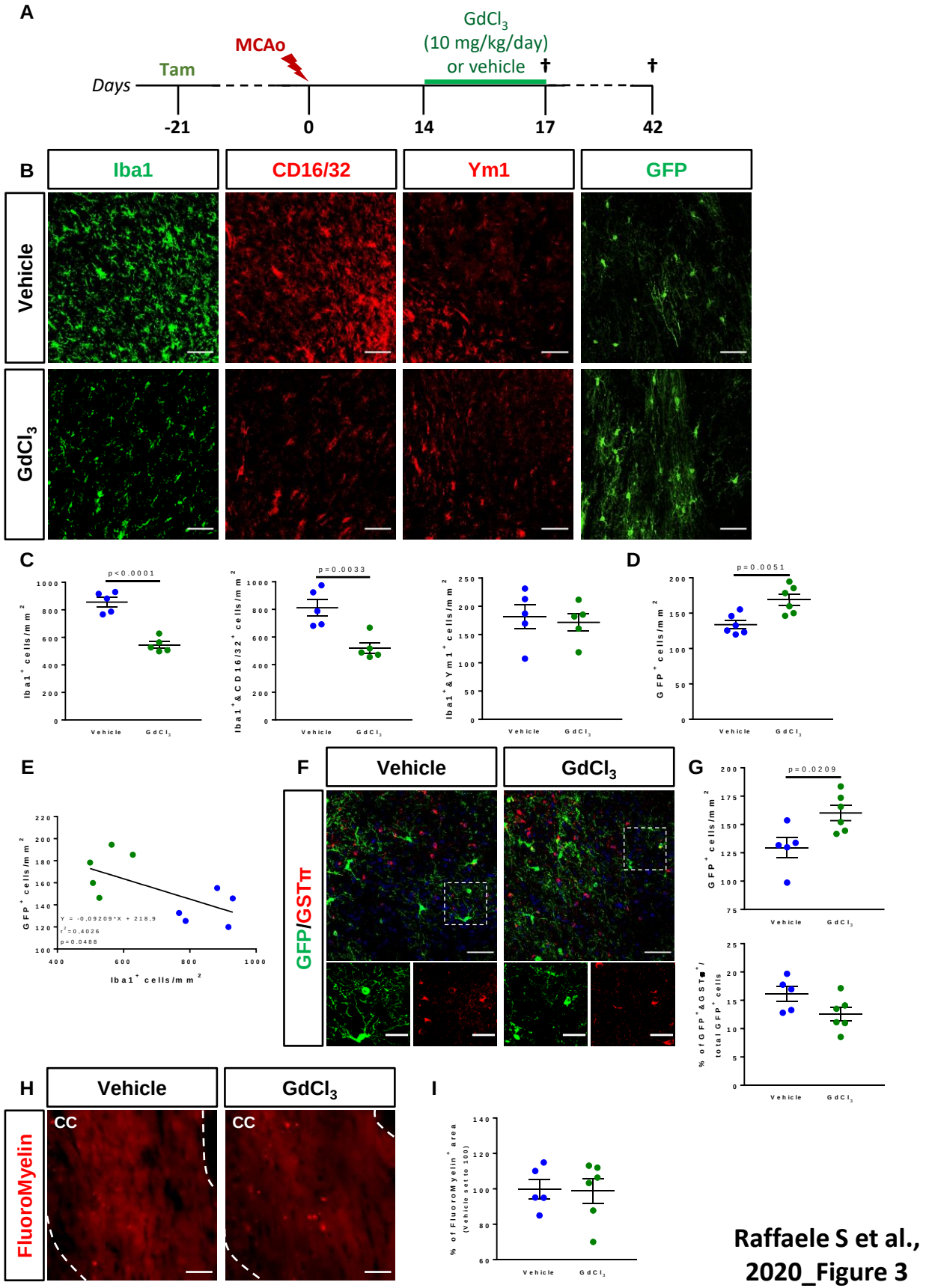

Raffaele S et al., 2020_Figure 3

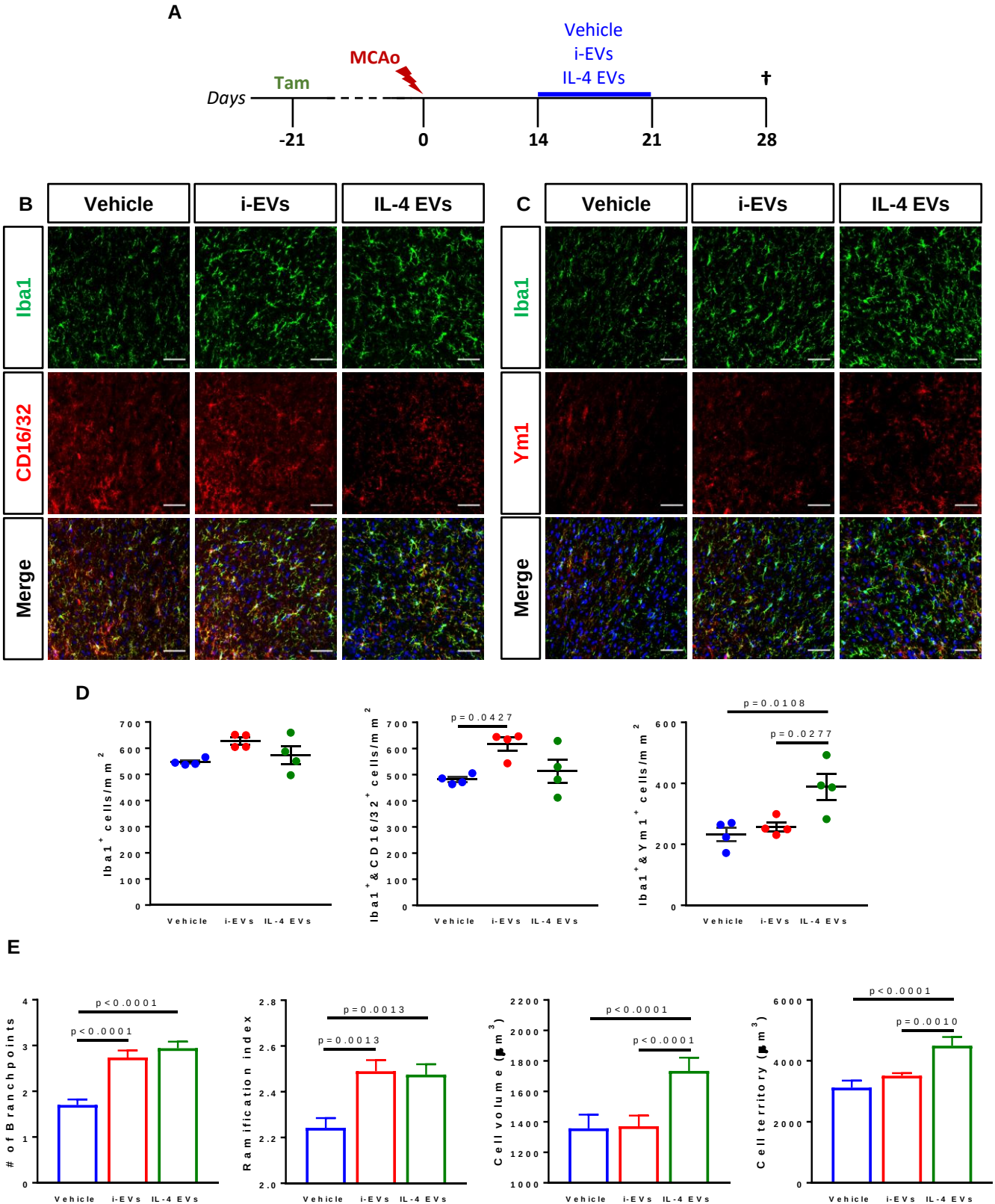

Raffaele S et al., 2020_Figure 4

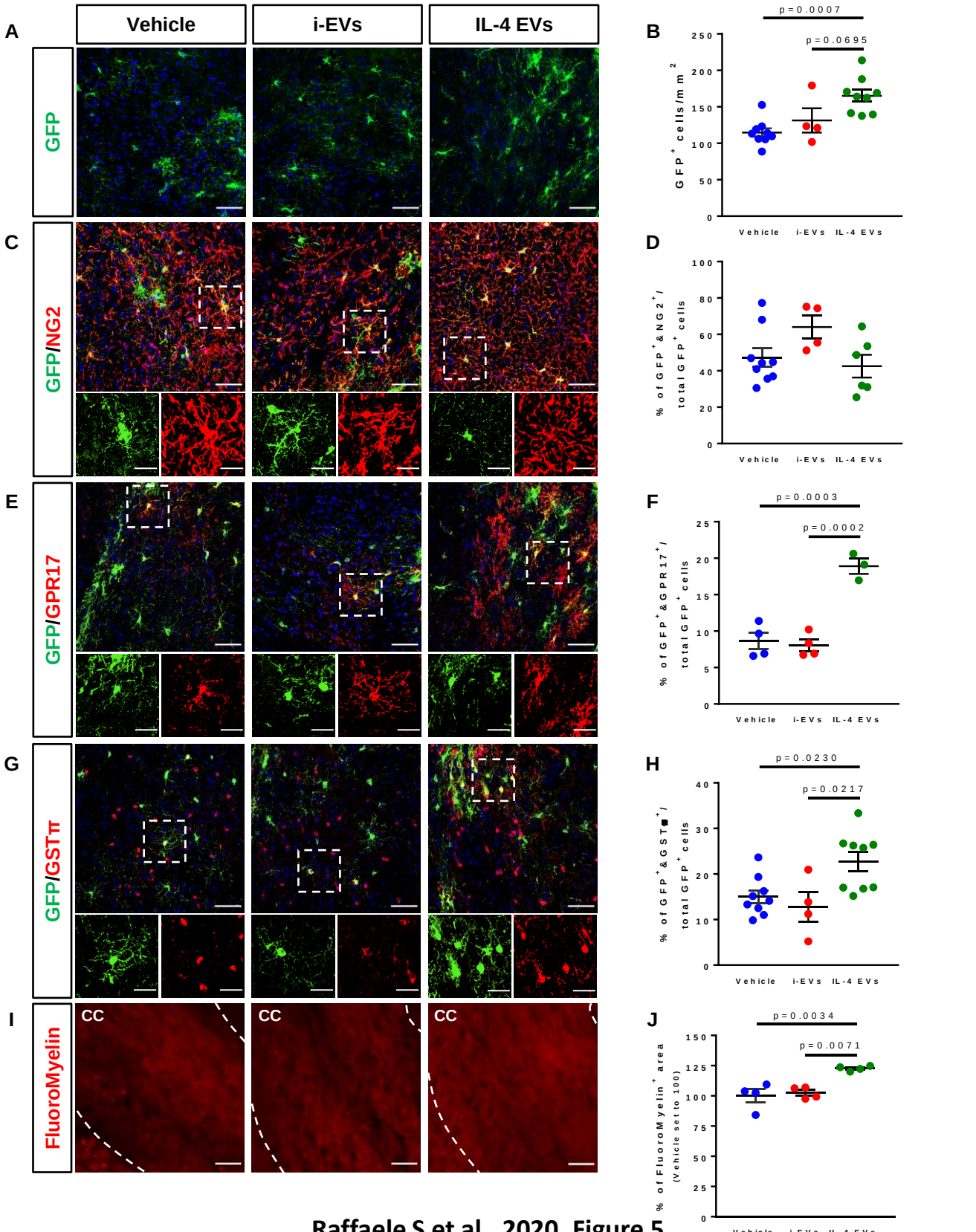

Raffaele S et al., 2020_Figure 5

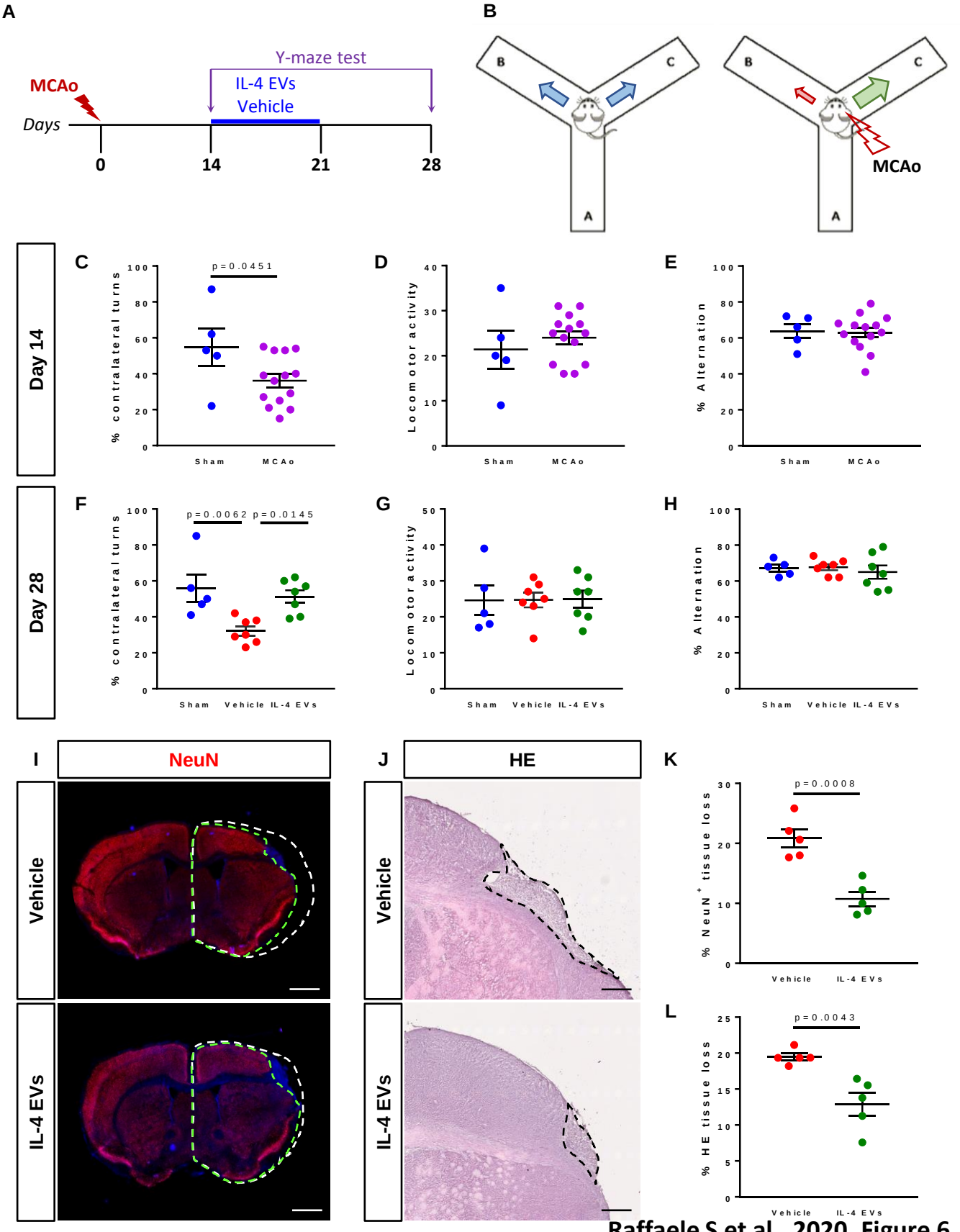

Raffaele S et al., 2020_Figure 6

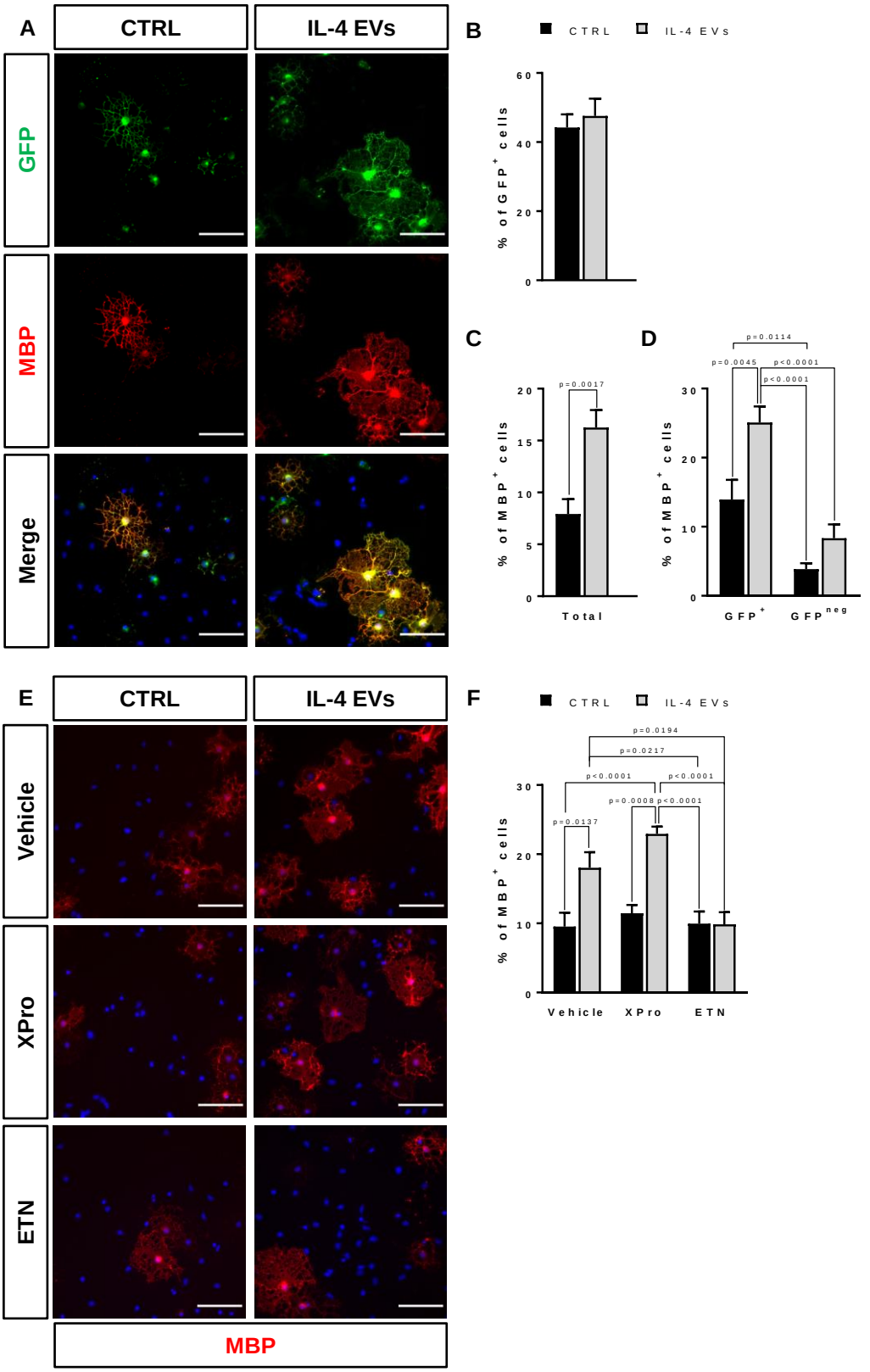

Raffaele S et al., 2020_Figure 7

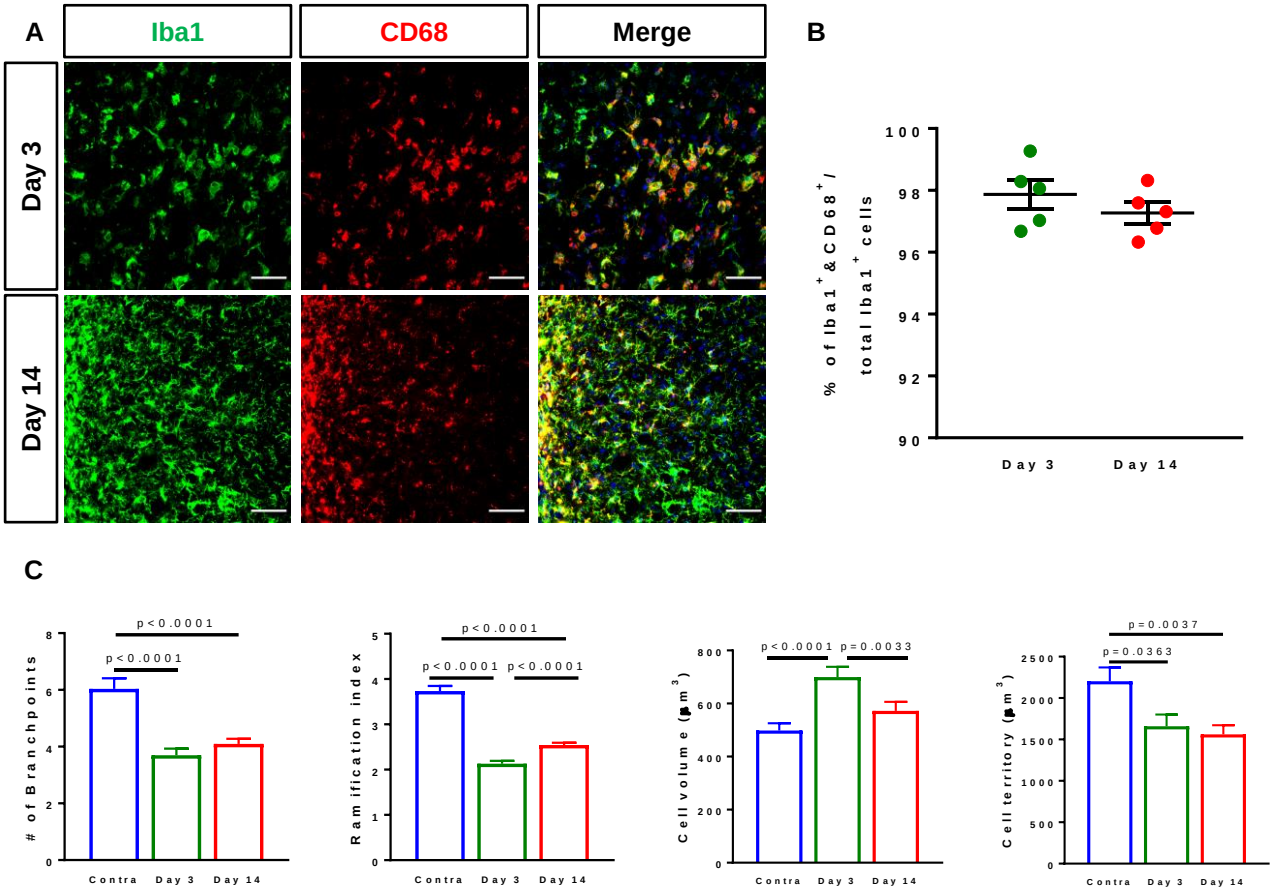

Figure S1. Iba1⁺ cells in the peri-infarct area express the scavenger receptor CD68 and undergo progressive morphological changes. (A) Representative images of Iba1⁺&CD68⁺ cells at the boundary of ischemic lesion (0-500 µm) at day 3 and 14 after MCAo. Scale bar: 50 µm. **(B)** Quantification of the percentage of Iba1⁺ cells co-expressing the scavenger receptor CD68 at the boundary of ischemic lesion (0-500 µm) at day 3 and 14 post-MCAo (n=5). Data are expressed as mean ± SE. **(C)** Quantification of Iba1⁺ cells number of branchpoints, ramification index, cell volume and cell territory at the boundary of ischemic lesion (0-500 µm) at day 3 and day 14 post-MCAo and in the corresponding region of the contralateral hemisphere at day 1 post-MCAo (130-150 cells from 3 animals/experimental condition have been analyzed). Data are expressed as mean ± SE. Kruskal-Wallis test followed by Dunn's post-hoc analysis.

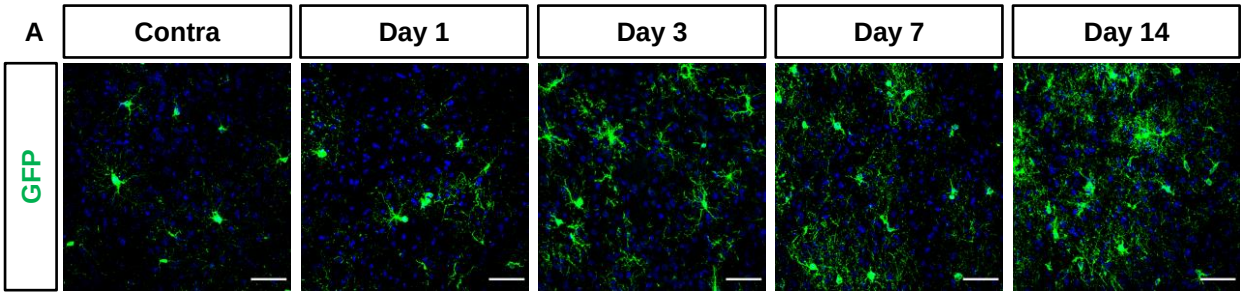

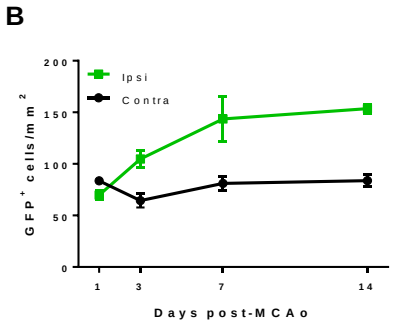

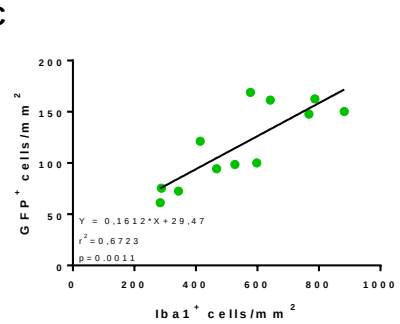

Ipsi vs Contra	p value
Day 1	ns
Day 3	0.0316
Day 7	0.0010
Day 14	0.0003

Days (ipsi)	p value
1 vs 3	ns
1 vs 7	0.0002
1 vs 14	<0.0001
3 vs 7	0.0459
3 vs 14	0.0103
7 vs 14	ns

Figure S2. GFP⁺ OPC density at injury borders increases over time after cerebral ischemia in parallel with microglia/macrophage activation. (A) Representative images of GFP⁺ OPCs at the boundary of ischemic lesion (0-500 µm) at day 1, 3, 7 and 14 after MCAo and in the corresponding region of the contralateral hemisphere at day 1 post-MCAo. Scale bar: 50 µm. **(B)** Quantification of the density of GFP⁺ OPCs at the boundary of ischemic lesion (0-500 µm) and in the corresponding region of the contralateral hemisphere at day 1, 3, 7 and 14 after MCAo (n=3). Data are expressed as mean ± SE. Two-way ANOVA (Interaction p=0.0017, Time p=0.0008, MCAo p<0.0001) followed by Tukey's post-hoc analysis (p values relative to multiple comparisons are reported in the tables). **(C)** Scatter plot representation of the linear correlation between the densities of Iba1⁺ cells (*x* axis) and GFP⁺ OPCs (*y* axis) at the boundary of ischemic lesion (0-500 µm) at the different time points analyzed after MCAo. For correlation analysis, two-tailed Pearson test was used.

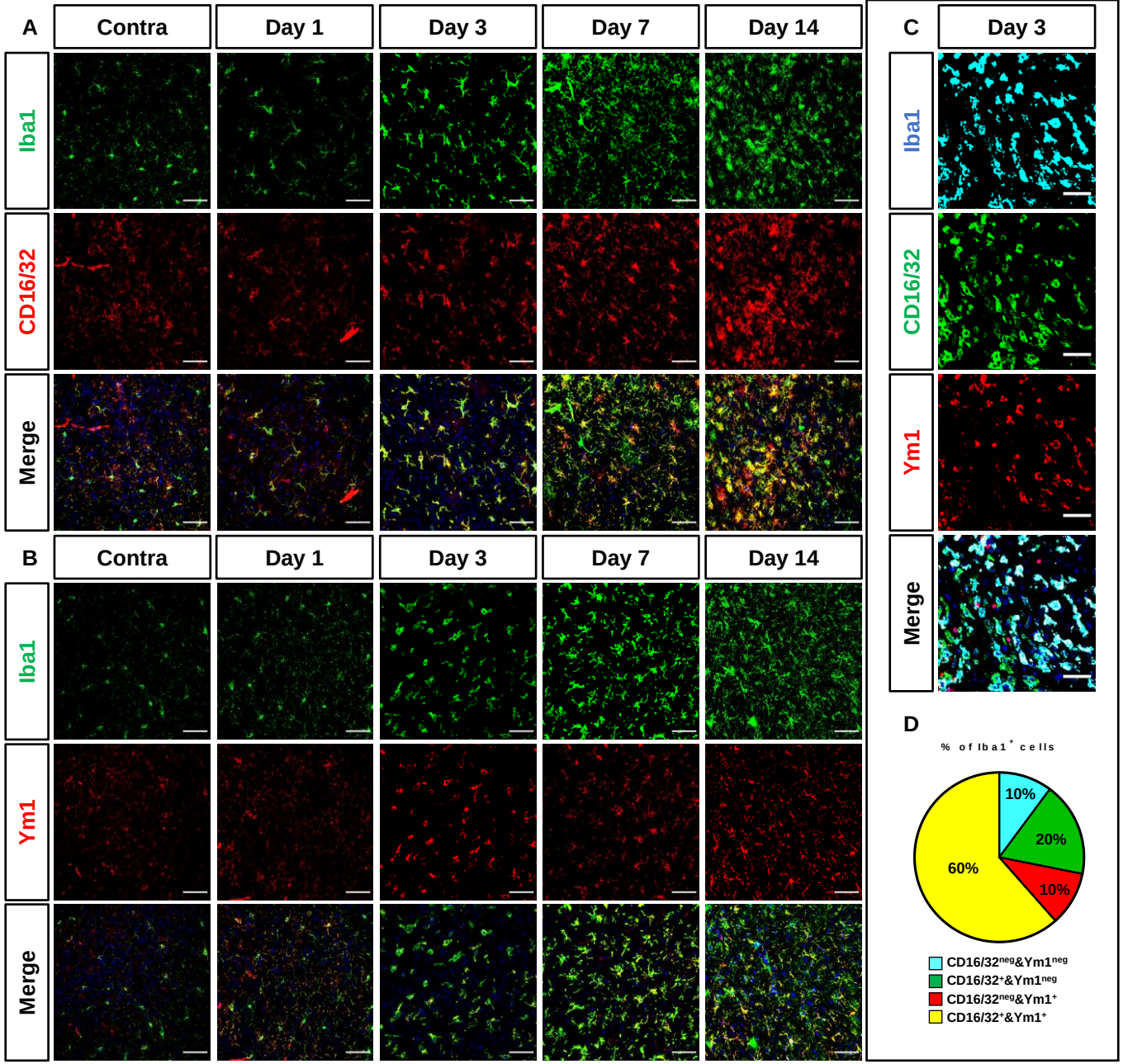

Figure S3. Characterization of Iba1⁺ co-localization with the pro-inflammatory marker CD16/32 or the pro-resolving factor Ym1 in the peri-infarct area. (A) Representative images of Iba1⁺&CD16/32⁺ cells at the boundary of ischemic lesion (0-500 µm) at day 1, 3, 7 and 14 after MCAo and in the corresponding region of the contralateral hemisphere at day 1 post-MCAo. Scale bar: 50 µm. **(B)** Representative images of Iba1⁺&Ym1⁺ cells at the boundary of ischemic lesion (0-500 µm) at day 1, 3, 7 and 14 after MCAo and in the corresponding region of the contralateral hemisphere at day 1 post-MCAo. Scale bar: 50 µm. **(C)** Representative images of triple positive Iba1⁺&CD16/32⁺&Ym1⁺ cells at the boundary of ischemic lesion (0-500 µm) at day 3 after MCAo. Scale bar: 50 µm. **(D)** Quantification of the percentage of Iba1⁺ cells co-expressing CD16/32, Ym1 or both markers at the boundary of ischemic lesion (0-500 µm) at day 3 after MCAo.

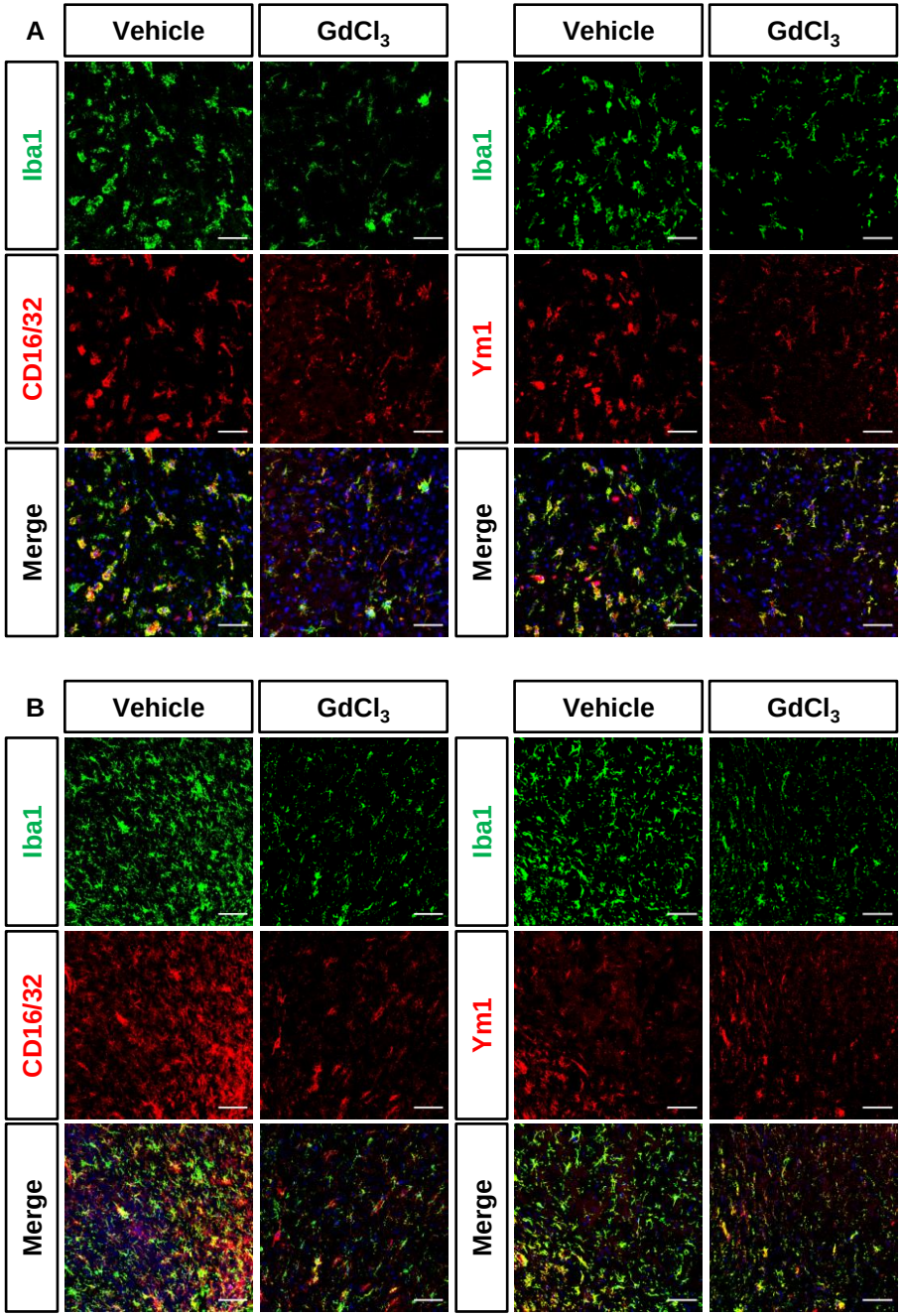

Figure S4. Characterization of Iba1 co-localization with CD16/32 or Ym1 after microglia/macrophage depletion during the early or late phase after MCAo. (A) Representative images of Iba1^{+}&CD16/32^{+} and Iba1^{+}&Ym1^{+} cells at the boundary of ischemic lesion (0-500 μm) at day 3 post-MCAo following intranasal administration of GdCl3 or vehicle. Scale bar: 50 μm. **(B)** Representative images of Iba1^{+}&CD16/32^{+} and Iba1^{+}&Ym1^{+} cells at the boundary of ischemic lesion (0-500 μm) at day 17 post-MCAo following intranasal administration of GdCl3 or vehicle. Scale bar: 50 μm.

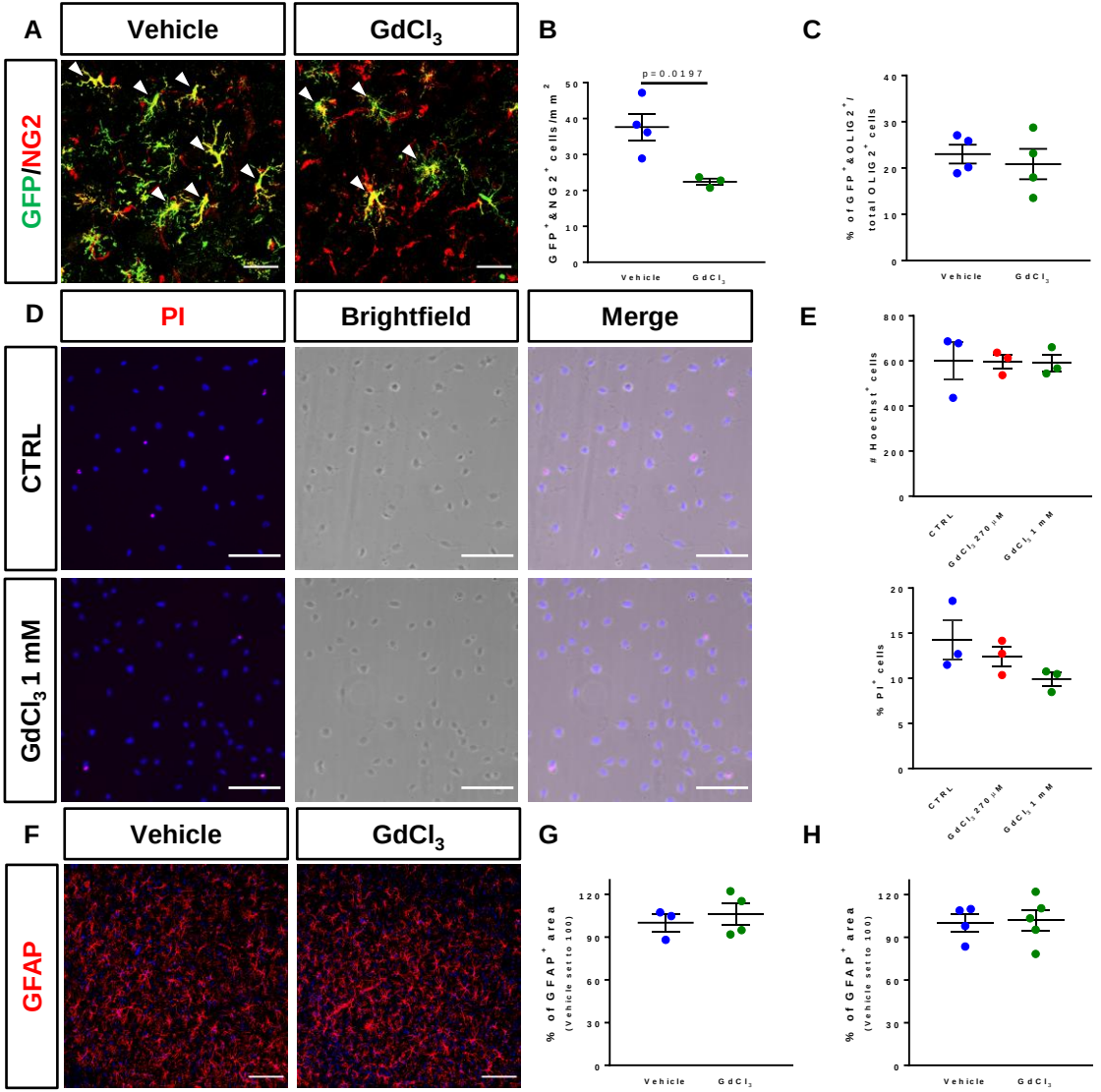

Figure S5. Microglia reduction by $GdCl_3$ treatment limits the recruitment of early GFP⁺ OPCs expressing NG2 at the boundary of ischemic lesion without exerting toxic effects on primary OPC cultures and on astrogliosis. (A) Representative images of GFP/NG2 staining at the boundary of ischemic lesion (0-500 µm) at day 3 post-MCAo following intranasal administration of $GdCl_3$ or vehicle. Arrowheads indicate cells co-expressing GFP and NG2. Scale bar: 50 µm. **(B)** Quantification of the density of $GFP^+\&NG2^+$ cells at the boundary of ischemic lesion at day 3 post-MCAo following intranasal administration of $GdCl_3$ or vehicle. Data are shown as mean ± SE (n=4-3). Student's t-test. **(C)** Quantification of the percentage of $Olig2^+$ cells labelled by GFP expression at the boundary of ischemic lesion at day 3 post-MCAo following early intranasal administration of $GdCl_3$ or vehicle (n=4). Data are expressed as mean ±SE. **(D)** Representative images of primary OPCs incorporating propidium iodide (PI) after treatment with $GdCl_3$ (1 mM) or medium alone (CTRL). Hoechst33258 was used to label cell nuclei. Scale bar: 50 µm. **(E)** Quantification of the number of $Hoechst33258^+$ cell nuclei and of the percentage of PI^+ apoptotic cell nuclei in primary OPC cultures exposed to $GdCl_3$ (270 µM or 1 mM) or CTRL. Data are shown as mean ± SE (n=3). **(F)** Representative images of GFAP staining at the boundary of ischemic lesion (0-500 µm) at day 3 post-MCAo following intranasal administration of $GdCl_3$ or vehicle. Scale bar: 100 µm. **(G)** Quantification of the percentage of $GFAP^+$ area at the boundary of ischemic lesion at day 3 post-MCAo following early intranasal administration of $GdCl_3$ or vehicle (n=3-4). Data are expressed as mean ±SE. **(H)** Quantification of the percentage of $GFAP^+$ area at the boundary of ischemic lesion at day 17 post-MCAo following late intranasal administration of $GdCl_3$ or vehicle (n=4-5). Data are expressed as mean ± SE.

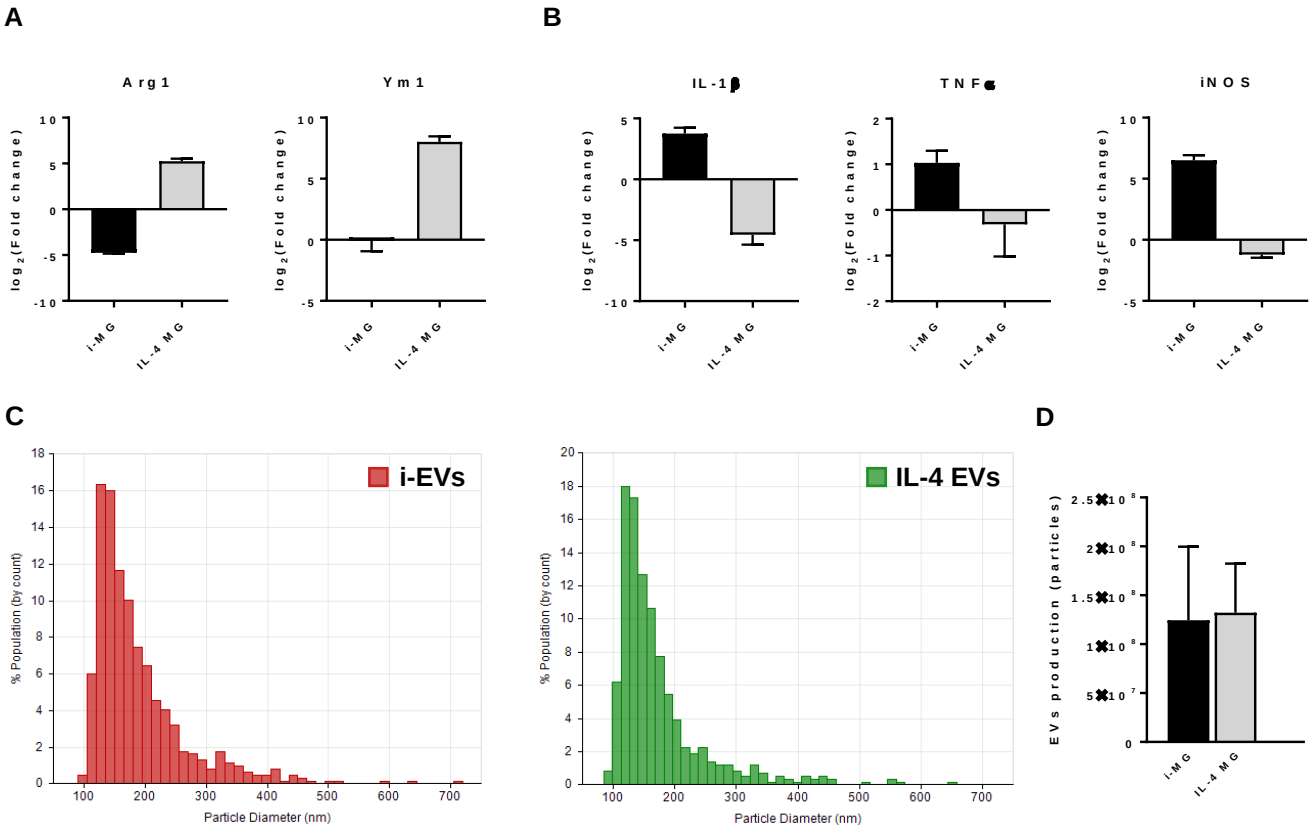

Figure S6. Characterization of polarization and EV release of murine microglia exposed to pro-inflammatory (i-MG) or pro-regenerative (IL-4 MG) stimuli. (A) Gene expression of pro-regenerative markers in primary microglia exposed to pro-inflammatory (i-MG) or pro-regenerative (IL-4 MG) stimuli with respect to non-stimulated cells (NS-MG) set to 0. Data are shown as mean ± SE. **(B)** Gene expression of pro-inflammatory markers in primary microglia exposed to pro-inflammatory (i-MG) or pro-regenerative (IL-4 MG) stimuli with respect to non-stimulated cells (NS-MG) set to 0. Data are shown as mean ± SE. **(C)** Size distribution graphs relative to EVs released by i-MG (i-EVs) and IL-4 MG (IL-4 EVs) upon ATP simulation. EV size was measured by Tunable Resistive Pulse Sensing (TRPS) technique. **(D)** Quantification of EVs produced by i-MG (i-EVs) and IL-4 MG (IL-4 EVs) upon ATP simulation. Data are expressed as mean ± SE.